PROCEEDINGS A

royalsocietypublishing.org/journal/rspa

Research

Cite this article: Grassia P, Torres-Ulloa C, Shokri N, Aryana S. 2025 Pressure-driven growth with forward and reverse foam flow: modelling foam flow in geological formations. *Proc. R. Soc. A* **481**: 20250042. https://doi.org/10.1098/rspa.2025.0042

Received: 15 January 2025
Accepted: 30 April 2025

Subject Areas:
mathematical modelling, fluid mechanics, applied mathematics

Keywords:
foam flow, porous media, seasonal gas storage, reverse flow, pressure-driven growth, mathematical modelling

Author for correspondence:
P. Grassia
e-mail: p.s.grassia@tue.nl

Pressure-driven growth with forward and reverse foam flow: modelling foam flow in geological formations

P. Grassia[1], C. Torres-Ulloa[2], N. Shokri[3] and S. Aryana[4]

[1]Department of Mechanical Engineering, TU Eindhoven, Groene Loper 3 AE Eindhoven 5612, The Netherlands
[2]Departamento de Ciencias Matemáticas y Físicas, Facultad de Ingeniería, Universidad Católica de Temuco, Rudecindo Ortega Temuco 03694, Chile
[3]Institute of Geo-Hydroinformatics, Hamburg University of Technology, Hamburg 21073, Germany
[4]Chemical and Biomedical Engineering, Dept. 3295, 1000 E. University Ave, Laramie, WY 82071, USA

PG, 0000-0001-5236-1850

The pressure-driven growth model is used to investigate the propagation of a foam front in a porous medium. Initially, the foam front moves forward due to an imposed gas injection pressure. Later, however, the injection pressure is reduced so that part of the front, deeper down in the medium, switches to reverse flow. The foam front is not, however, predicted to retrace its original path. Along most of its length moreover, the reverse flow front is predicted to move surprisingly quickly, which also affects the total area swept out. On the other hand, some parts of the front very close to the bottom move only slowly in reverse flow, such that the front is predicted to develop a kinked shape. Perturbations superposed on the front shape can also cause it to develop sharp concave corners. Overall, the findings enhance the understanding of foam behaviour in porous media, when sudden changes in flow direction occur during the course of the flow.

Electronic supplementary material is available online at https://doi.org/10.6084/m9.figshare.c.7819490.

THE ROYAL SOCIETY PUBLISHING

1. Introduction

There are numerous scenarios which involve foamed gas displacing liquids in porous media. These include, e.g. foam improved oil recovery [1–4], soil remediation [5–9] and aquifer remediation [9–12]. These applications rely on the surprisingly low mobility of foamed gas in porous media, or equivalently the surprisingly high resistance to flow of foamed gas. Indeed, foamed gas is not only orders of magnitude more resistant to flow than unfoamed gas, it can also be more resistant to flow than the original liquids present in a medium [13–17]. Foam can thereby act as an effective blocking agent preventing or at least significantly reducing flow from one part of a medium to another, especially in the presence of heterogeneities [18]. This can for instance prevent the spread of contaminants in a medium [19,20]. Conversely, controlling the flow [21–23] of the least mobile fluid (i.e. foamed gas) present in a medium also controls the flow of all other fluids present.

In the context of mitigating climate change, there is much interest in capturing carbon dioxide and injecting it into porous media for storage [24,25]. It has been proposed [24–26] that foaming CO_2 could be part of the strategy for directing it into media in a controlled fashion, and also for maintaining it *in situ*. However, questions then arise [27,28] as to what might happen if one begins to inject at a reduced rate (e.g. by reducing an injection pressure). This may need to be done deliberately (e.g. to manage changes in throughput in response to downhole pressure build up and to prevent fracturing rock [29] which could otherwise lead to CO_2 escape). It may also happen unplanned (e.g. due to pump failure or a reduction in the performance of a pumping system). In an extreme case, further injection might be stopped altogether and thereafter the system is shut in [27]. It is then relevant to ask how foamed CO_2 already in a medium would continue to flow and redistribute in situations like this. Similar questions could arise for temporary seasonal storage of other gases, e.g. green hydrogen [30,31]. Foamed gas could be stored in a porous medium (e.g. a geological formation). For the gas to be used, however, eventually injection would need to stop and extraction would begin. It is interesting then to ask from which parts of the medium gas would be extracted, and in which parts of the medium it would remain. These then are the sorts of questions that will be addressed here.

Tackling questions like these, so as to understand how a reduction of injection pressure affects flow behaviour of foamed gas and liquid in a large-scale porous medium, typically requires a Darcy-type model for the fluid flow fields throughout the entire medium [32–36]. This needs to be coupled to a foam model, describing how much less mobile (sometimes orders of magnitude less mobile) foamed gas is compared to unfoamed gas [13–17]. A phase transport equation (i.e. a conservation equation for foamed gas and for liquid) is also required, again throughout the entire medium [32–36]. Models containing all these various ingredients can be quite involved to implement numerically [32–36]. There is, however, a simpler alternative, namely, the pressure-driven growth model [29,37,38]. This is a special case of Darcy's Law which, under certain conditions and limitations to be described later, approximates how a foam front might propagate inside a medium [29,37–46]. Pressure-driven growth is quick and simple to implement, because it aims to describe just the foam front, not the entire medium. It can also be implemented easily in cases with heterogeneous and/or anisotropic media [41,42,44], although attention often has focused on homogeneous and isotropic systems [38,43,45]. Prior work on pressure-driven growth has, however, been restricted to fronts that propagate forward without suffering any reduction in driving injection pressure [29,37,38]. This is despite the fact that the physical ingredients necessary to extend pressure-driven growth to a case involving a reduction in driving pressure have already been determined [27,28]. The ingredients are available, but the extension to the model has not been implemented. Hence, if a reduction in injection pressure were to occur, the interesting questions of what might be predicted to happen to a foam front have not been addressed. Implementing the model for this case and tackling these questions is therefore the novel contribution of the present work.

In §2, we review the pressure-driven growth model and review also how to extend it to the case of a reduction in imposed pressure. The discussion in §2 focuses on the physics of the model.

Mathematical details are deferred until §3. After that, in §4, we analyse the model and discuss what it predicts in general terms. Then, in §5, we present simulation results for the model. Finally, in §6, we provide the conclusion.

2. Review of pressure-driven growth

In what follows, we first review the pressure-driven growth model, in the first instance without contemplating any reduction in driving pressure (§2a). Readers already familiar with relevant literature [29,37–46] may prefer to skip this material. Then, in §2b, we review literature on the extension of pressure-driven growth accounting for a reduction in injection pressure [27,28]. Not only is reduction in driving pressure interesting in the context of applications (e.g. gas storage in porous media as already mentioned above), it also turns out to be of inherent interest in the context of the physics of the pressure-driven model itself. This aspect is also discussed in §2b helping also to motivate the study.

(a) Pressure-driven growth considering only forward flow

The situation modelled by pressure-driven growth [29,37–46] is as follows (see figure 1a which considers a two-dimensional system for simplicity, although generalization to an axisymmetric case is possible [29]). Gas is injected into a medium already filled with liquid containing surfactant. In other words, a slug of gas is injected after injection of a large slug of surfactant liquid. Foam forms *in situ*. Specifically, there is a foam front which propagates forward with finely textured foam immediately upstream, and coarsely textured foam located farther back. Downstream of the foam front there is liquid (i.e. surfactant solution) that was present initially throughout, but which has now been partially displaced by the foam.

Based on established foam mobility models [13–17], the mobility of the finely textured foam is expected be significantly lower than that of either the coarsely textured foam or the initial liquid. Since Darcy's Law [32–36] predicts that pressure gradients scale inversely with mobility, it follows that dissipative pressure drops occur predominantly in the finely textured, low mobility region. Thus, once the foam front is quite some distance away from the point of injection, significant dissipative pressure drops occur away from the injection region. This is noteworthy, since in the case of axisymmetric injection, on geometric grounds, the highest velocities necessarily occur close to the point of injection. The presence of foam means that the largest pressure gradients no longer need to coincide with the highest velocities. Here, however, we elect to solve a Cartesian system rather than an axisymmetric one, so it is definitely near the foam front where the largest pressure gradients are anticipated. It is also assumed that (as drawn in figure 1a) the finely textured foam occupies a region much thinner than the overall displacement distance that the front has advanced. Thus, any dissipative pressure drop is assumed to be confined now near the low-mobility foam front, although it is possible to query this assumption [28,47] as we discuss later: see §2b and also electronic supplementary material fig. S2 in the appendix.

Darcy's Law also predicts [32–36] that front speed is proportional to the magnitude of pressure gradient at the front. Provided an estimate is available of the assumed small but finite thickness of the low-mobility foam at the front (discussed further in electronic supplementary material, section A in the appendix), it is possible to relate pressure gradient to pressure drop. Hence, front speed is proportional to the pressure drop across the low-mobility foam front. The pressure drop is then estimated as the difference between the driving injection pressure of the gas upstream and the hydrostatic pressure in the liquid downstream (with hydrostatic pressure in the gas upstream being neglected compared to that in the downstream liquid). This estimate of pressure drop is consistent with ignoring any dissipative pressures away from the front. It is this proportionality between front speed and the estimated pressure drop which defines the pressure-driven growth model [29,38].

Since the hydrostatic pressure in the liquid grows with depth, there is a well-defined depth at which injection pressure and hydrostatic pressure balance. This is then the maximum depth

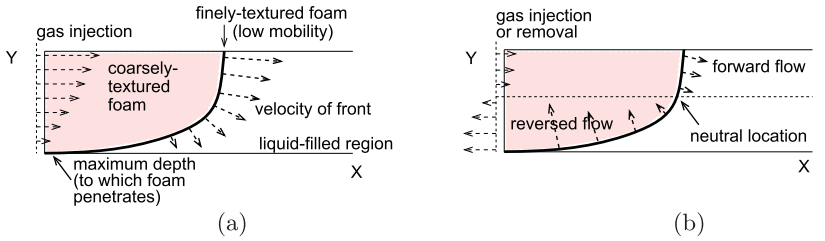

Figure 1. Situation modelled by pressure-driven growth (a) forward flow (b) forward and reverse flow. A Cartesian system is assumed in which the coordinate *X* is horizontal and *Y* is vertical.

to which gas can penetrate. Moving upwards from this maximum depth, the speed of the foam front grows. Those parts of the foam front that are higher up thereby displace farther [29,38]. As a result the front normal, which is also the direction of front propagation, points both to the right and downwards, as indicated by the direction of arrows drawn on figure 1a. In other words, a front moving to the right and downwards is considered to be undergoing forward flow.

To summarize, pressure-driven growth represents a simple, special case of Darcy flow for foam in porous media [29,38]. It is, however, subject to a limitation that dissipation is assumed to arise entirely from a thin region of finely textured foam at the foam front.

(b) Pressure-driven growth in forward and reverse flow

Thus far we have only described pressure-driven growth for injection into a system with no reduction in pressure, which has been considered in numerous prior studies [29,37–46]. However, we have not yet considered the effect of reducing the driving injection pressure, which is the specific question to be addressed here, as discussed in what follows.

After a sudden reduction in driving pressure, there will be an upwards shift in the location at which driving pressure and hydrostatic pressure balance. This will be called the neutral location. It is indicated by a dashed line in figure 1b. Above the neutral location, gas continues to be injected and the foam front still propagates forward, albeit less quickly than before. Below the neutral location, however, the foam front moves in the opposite direction, i.e. upwards and to the left as figure 1b shows. Hence, this part of the foam front at least undergoes reverse flow [27,28]. Since some parts of the front are still moving forwards, and other parts are moving in reverse, it unclear *a priori* whether there is net injection or net extraction of gas.

The front speed depends now on the height difference between any selected location and the neutral location. However, it also depends on whether the mobility of foamed gas in reverse flow is the same as or different from that in forward flow. In fact, prior work [27,28] has found that the forward and reverse mobilities turn out to be rather different, as §3 goes on to explain. What that prior work achieved [27,28] was to formulate a two-dimensional pressure-driven growth model for foamed gas in forward and reverse flow. It also determined (based on one-dimensional fractional flow theory [47–50] along flow paths) the parameter values for front mobilities to be inserted into that model, still subject to the limitation that dissipation is assumed to arise entirely from finely textured foam neighbouring the foam front. However, as already alluded to, the model itself was never actually solved. The novel contribution of the present work is to obtain solutions of the model, analyse them, and thereby gain insight into how foam fronts reconfigure when driving injection pressures are reduced.

One particularly interesting aspect of figure 1b is that, below the neutral location, the front shape (as viewed from the region into which the front is propagating) is concave, whereas elsewhere in figure 1b (and in figure 1a), it is convex. Concave regions in particular warrant special attention, as they can be challenging to handle in the context of pressure-driven growth. This is because concavities have the potential to focus into sharp concave corners [38,43,45].

Physically, a sharp corner implies that the front reorients not over a length scale comparable to the total propagation distance, but rather over an assumed somewhat smaller distance, corresponding to the thickness of the low-mobility foam region at the front. However, the presence of a concavity does not necessarily guarantee the formation of a sharp corner, as focusing only occurs if the front travels a sufficient distance within the concave region [42,44]. Later on in this work, we explore, under various conditions, whether or not sharp corners develop.

One caveat here is that, even after the onset of reverse flow, we continue to assume that low mobilities are confined to a small region of space. Actually, this assumption has been queried in the literature [28,47]. The issue is that, even when low mobilities are confined to a small domain of liquid saturations near the saturation at a foam front [27], this need not correspond to a small domain in space (see electronic supplementary material, fig. S2 in the appendix). The issue arises both in forward flow and in reverse flow [28]. However, reverse flow exacerbates it: when surfactant liquid is driven towards (or equivalently re-invades) a region of foamed gas, low mobilities can occupy a really quite significant region of space [28,47], a fact that can be exploited in well-stimulation treatments in a petroleum engineering context [51,52]. This, however, also calls into question the validity of the model used here. That said, the model can tolerate moderate increases in the thickness of the region over which low mobilities occur. All this does is to slow down the speed at which the foam front moves [38], and hence extend the time scales for foam front evolution (see electronic supplementary material, section A(c) in the appendix for explanation). We work in terms of dimensionless variables, which results in these effects being scaled out.

Understanding the mobilities that arise in a geological formation when liquid surfactant solution re-invades a region filled with foamed gas [47] remains a challenging topic. It is possible for instance that, during such a process, some of the gas from within the foam might dissolve into the surfactant solution [53]. Furthermore, gas might also migrate vertically out of the foam swept region. This gas might then be replaced by liquid (e.g. brine) from regions which the surfactant has yet to reach, affecting in turn foam stability and foam mobility [53]. Effects like these are, however, excluded from the simplified model for foam front mobility that will be used here.

3. Mathematical model and governing equations

The previous section focused on pressure-driven growth from a physical point of view. The present section provides a more mathematical point of view, including governing equations.

As already explained, pressure-driven growth aims to model not the entire medium as a Darcy model would [32–36], but instead just the foam front. Mathematically, the front is represented by a curve across which the liquid fraction (also called liquid saturation) exhibits a discontinuity. This can be a discontinuous jump between finely textured foam and pure liquid (in the case of forward flow) [29,38], but a more general discontinuity in the case of reverse flow (as will be explained shortly) [27]. Either way, it is the propagation of this discontinuity that we are aiming to track. Pressure-driven growth is therefore expressed as a Lagrangian model for front 'material points', i.e. points that are advancing at the same velocity as the discontinuity. The evolution of the front shape is then deduced by discretizing the front into a collection of such material points, and following the trajectories of all those points [38].

(a) Dimensionless equations: forward flow

In this section and the next one, we present the equations that govern how the shape of the foam front evolves with time. We work in dimensionless form. The original dimensional equations [29,38] are presented in electronic supplementary material, section A in the appendix. One unit of dimensionless distance represents the vertical extent over which the foam front can penetrate. In addition, as we will see, half a unit of dimensionless time corresponds to the time after which the foam front has propagated horizontally farther than it can propagate vertically [38]. In applications involving gas storage in geological porous media, buoyancy sets a limit on vertical

penetration of foam. Hence, foam is expected to propagate farther horizontally than vertically (as e.g. figure 1 shows). Typically, therefore, we are interested in an evolution of up to several units of dimensionless time.

To provide a sense of scale [29,38], in a typical field application, one unit of dimensionless distance might correspond to approximately 100 m whereas a unit of dimensionless time might be up to the order of months, which seems compatible with seasonal storage of an energy carrying gas. These estimates (see electronic supplementary material, section A(c) in the appendix for details) are based on gas injection at a pressure of approximately 10 atm above the pressure of a geological porous medium, although the medium itself might already be at a significantly elevated pressure relative to atmospheric conditions. Injecting at a lower pressure difference between the gas and the medium would reduce proportionally both the unit of distance and the unit of time (see electronic supplementary material, section A9c). Consequently, the front would need less dimensional time to sweep a unit of dimensionless area. However, this would now correspond to a much smaller dimensional area being swept, as the unit of distance is reduced both vertically and horizontally. Thus, much less gas would be stored.

The dimensionless equations for pressure-driven growth in forward flow become

$$\frac{\mathrm{d}\boldsymbol{X}}{\mathrm{d}\tau} = \frac{Y}{s}\boldsymbol{n} \tag{3.1}$$

and

$$\frac{\mathrm{d}s}{\mathrm{d}\tau} = \boldsymbol{n}.\frac{\mathrm{d}\boldsymbol{X}}{\mathrm{d}\tau}. \tag{3.2}$$

Here, $\boldsymbol{X} \equiv (X, Y)$ is the dimensionless position of a Lagrangian material point on the foam front, s is the dimensionless distance which it has displaced during injection and τ is dimensionless time. Also, $\boldsymbol{n}$ is the front normal, which is obtained by considering adjacent points that are also on the foam front. For the solution domain, we are interested in values of Y satisfying $0 \leq Y \leq 1$, and values of X, s and τ, satisfying, respectively, $X \geq 0$, $s > 0$ and $\tau \geq 0$.

The factor Y in the numerator on the right-hand side of equation (3.1) is a measure of how much an imposed injection pressure in the gas is able to overcome a hydrostatic pressure in the liquid which the gas is attempting to displace. At the bottom $Y = 0$, for instance, the imposed injection pressure is completely counterbalanced by hydrostatic pressure, and the front cannot move. The factor s in the denominator of the right-hand side of equation (3.1) is a manifestation of the thickness of a low-mobility foam front growing proportionally with the distance through which the foam front as a whole has moved. This in turn increases the resistance to flow, and so causes the front to slow down over time. Note that the low-mobility foam front is considered thin, so its thickness is certainly not equal to the displaced distance, but instead is proportional to it (see electronic supplementary material, section A(a) in the appendix for more explanation). However, the proportionality coefficient has been hidden by the scaling used in the dimensionless formulation (see electronic supplementary material, section A(c)). As written, equation (3.1) assumes a homogeneous and isotropic medium, although extending to a medium that is heterogeneous and/or anisotropic is possible [41,42,44] (see electronic supplementary material, section A(a)).

Equations (3.1)–(3.2) need to be solved with a boundary condition, namely, that at $Y = 1$; flow is along the top boundary, and hence the front normal satisfies $\boldsymbol{n} = (1, 0)$ there. The equations also need to be solved with an initial condition at $\tau = 0$, which is that the front is initially vertical, i.e. $X = 0$ for all Y at time $\tau = 0$. An initial condition for s is also needed. One option is to select $s = 0$ initially for all points on the front, but that is awkward numerically [38], as s appears in the denominator of the above mentioned equations. We therefore select instead $s = s_0$ initially, where $s_0 > 0$ here is an arbitrarily chosen small but finite value. We choose $s_0 = 0.001$, but the exact choice is relatively unimportant [38]: once s has grown to become rather larger than s_0, solutions cease to be sensitive to s_0.

Via the boundary condition, it is possible to predict using equation (3.2) that at the top of the front (i.e. at $Y = 1$), $\mathrm{d}s/\mathrm{d}\tau = \mathrm{d}X/\mathrm{d}\tau$. Thus at the top boundary, $s = X + s_0$. Once s and X have

grown significantly larger than s_0, we have to a good approximation $s \approx X$ at the top boundary. It then follows via equation (3.1) that $X \approx s \approx (2\tau)^{1/2}$ at $Y = 1$. This then explains why, as already mentioned, half a unit of dimensionless time corresponds to displacing horizontally one unit of dimensionless distance [37,38].

The dimensionless mathematical model for forward flow is now specified. Dimensionless equations incorporating reverse flow are described next.

(b) Dimensionless equations forward and reverse flow

If after a certain time, an imposed driving pressure is reduced, we have already mentioned that some parts of the front continue moving forward (points above the dashed line in figure 1b), whereas other parts of the front undergo reverse flow (points below the dashed line in figure 1b). The equation for forward flow involves only a minor modification relative to equation (3.1), namely,

$$\frac{\mathrm{d}\boldsymbol{X}}{\mathrm{d}\tau} = \frac{(Y - Y_{\mathrm{neut}})}{s}\,\boldsymbol{n}, \tag{3.3}$$

where Y_{neut}, satisfying $0 < Y_{\mathrm{neut}} \leq 1$, denotes the neutral location, in other words it represents the location of the dashed line in figure 1b. Physically, Y_{neut} represents the relative amount by which pressure has been reduced. For example, selecting $Y_{\mathrm{neut}} = 0.5$ corresponds to halving the amount that the driving pressure for the flow exceeds the pressure within the geological porous medium. Equation (3.3) applies for $Y \geq Y_{\mathrm{neut}}$. Here, the factor $(Y - Y_{\mathrm{neut}})$ represents a dimensionless difference between an imposed driving pressure in the gas and a hydrostatic pressure in the liquid, but accounting for the fact that the gas pressure is no longer as large as before. Thus, the velocity predicted by equation (3.3) is clearly less than that predicted by equation (3.1), and indeed a point at the neutral location $Y = Y_{\mathrm{neut}}$ ceases to move altogether.

In the case of reverse flow, we have instead

$$\frac{\mathrm{d}\boldsymbol{X}}{\mathrm{d}\tau} = \frac{|Y - Y_{\mathrm{neut}}|}{(\max(s_{\mathrm{switch}} - s_{\mathrm{since}}, 0) + M_{\mathrm{fwd/rev}}\, s_{\mathrm{since}})} \left(\frac{\Delta f_l}{\Delta S_l}\right)_{\mathrm{rev/fwd}} \boldsymbol{n}, \tag{3.4}$$

which applies for $Y \leq Y_{\mathrm{neut}}$, such that again a point at $Y = Y_{\mathrm{neut}}$ ceases to move altogether. Here, s_{switch} is the value of displaced distance s which a material point had accumulated while originally moving forwards, up to the instant at which pressure was reduced so that the point switched direction and began flow reversal. Also, $M_{\mathrm{fwd/rev}}$ is a ratio of mobilities (to be explained shortly; see also electronic supplementary material, fig. S1c–d in the appendix), and $(\Delta f_l/\Delta S_l)_{\mathrm{rev/fwd}}$ (again to be explained shortly) is a ratio involving a jump in a quantity known as fractional flow f_l and a jump in liquid saturation S_l (further details can be found in electronic supplementary material, fig. S1a–b in the appendix). In addition, s_{since} is the distance that a point has displaced since flow reversal began, which satisfies (analogously to equation (3.2))

$$\frac{\mathrm{d}s_{\mathrm{since}}}{\mathrm{d}\tau} = \boldsymbol{n}.\frac{\mathrm{d}\boldsymbol{X}}{\mathrm{d}\tau}. \tag{3.5}$$

This equation requires an initial condition at the time denoted τ_{switch} at which flow reverses. This time τ_{switch} will be referred to as the switching time. Compatible with the initial condition used in equation (3.2), we set $s_{\mathrm{since}} = s_0$ when $\tau = \tau_{\mathrm{switch}}$. As mentioned earlier, s_0 is an arbitrarily chosen small but finite value (with the value $s_0 = 0.001$ selected here). Once s_{since} has grown rather larger than s_0, solutions cease to be sensitive to s_0. A boundary condition is also imposed that the front is mirror symmetric about the Y-axis, i.e. figure 1b shows just half of the mirror symmetric shape. Note that during reverse flow, it is considered that the front normal $\boldsymbol{n}$ has switched direction, i.e. below the dashed line in figure 1b, the front normal $\boldsymbol{n}$ tends to point upwards and also to the left. On the Y-axis, however, mirror symmetry requires that $\boldsymbol{n} = (0, 1)$. The aforementioned switch in direction of $\boldsymbol{n}$ explains why an absolute value is used in the term $|Y - Y_{\mathrm{neut}}|$ in equation (3.4): as discussed already, this term represents a difference between liquid hydrostatic pressure and imposed driving pressure in the gas. Other terms appearing within equation (3.4) are described in the following sections.

Table 1. For the foam model employed here, ratios of parameters during forward flow and during reverse flow as used in equation (3.4) or analogously in equations (3.6)–(3.7).

$M_{\mathrm{fwd/rev}}$	$(\Delta f_l/\Delta S_l)_{\mathrm{rev},0/\mathrm{fwd}}$	$(\Delta f_l/\Delta S_l)_{\mathrm{rev},\infty/\mathrm{fwd}}$
29.4	11.4	1.97

(c) Resistance to flow

Equations (3.1) and (3.3) have just a single term s in the denominator (representing resistance to flow presented by the foam front). By contrast, the denominator of equation (3.4) contains (at least in the case for which $s_{\mathrm{since}} < s_{\mathrm{switch}}$) a sum of two terms $s_{\mathrm{switch}} - s_{\mathrm{since}}$ and $s_{\mathrm{since}}\, M_{\mathrm{fwd/rev}}$. This sum in the denominator follows from the nature of the front in reverse flow [27]. As mentioned already, the front is a discontinuity in liquid saturation which we try to track. However, there is no longer a jump from a saturation corresponding to finely textured, low-mobility foam on one side to pure liquid on the other. Instead, as will be explained below, there is a jump in saturation from a finely textured low-mobility foam on one side to another finely textured, low-mobility foam (but with slightly higher saturation and even lower mobility) on the other [27]. The terms in the denominator of equation (3.4) represent the sum in series of the resistance to flow offered by each of these regions.

Specifically, the term $s_{\mathrm{switch}} - s_{\mathrm{since}}$ represents the resistance to flow from the region above and to the left of the foam front in figure 1b, i.e. in what is now the downstream direction [27]. It turns out to be at the same liquid saturation as is found immediately above and to the left of a front undergoing forward motion. In reverse motion, however, this region starts to be consumed as the front moves. It thereby becomes thinner over time (as can be seen in electronic supplementary material, fig. S2 in the appendix), and so presents less resistance to the flow [27]. This explains the rationale for having a term involving $s_{\mathrm{switch}} - s_{\mathrm{since}}$ which decreases as s_{since} increases. We emphasize that finely textured foam is found in what is, at least by assumption, a thin region close to the front. We are not claiming that it extends over an entire region of size $s_{\mathrm{switch}} - s_{\mathrm{since}}$, but instead could correspond to a thinner region of size proportional to that. However, as also happened in the equations within §3a, the proportionality coefficient has been hidden in the scalings used in the dimensionless equations (see electronic supplementary material, section A(c) in the appendix for details).

The term $M_{\mathrm{fwd/rev}}\, s_{\mathrm{since}}$ within equation (3.4) also represents resistance associated with a region of finely textured, low-mobility foam which is below and to the right of the front in figure 1b, i.e. it is upstream of the front. This is newly formed when the front begins reverse flow [27], and it grows in size as the front moves and hence as s_{since} increases. Using fractional flow theory, it is possible to predict (as already alluded to) that this upstream region is at slightly higher liquid saturation and also has significantly lower mobility than the downstream region [27] (see electronic supplementary material, table S1 in the appendix for details, with a summary in table 1). The value $M_{\mathrm{fwd/rev}}$ is the ratio of the downstream mobility (i.e. the one that appears also in forward flow) to the upstream mobility (i.e. the one that appears only in reverse flow). This then is a quantity rather greater than unity (see table 1, and in addition electronic supplementary material, fig. S1c–d in the appendix). Given the low mobility on the upstream side, the front does not need to propagate far at all before the resistance associated with the foam upstream $M_{\mathrm{fwd/rev}}\, s_{\mathrm{since}}$ begins to dominate that from the foam downstream $s_{\mathrm{switch}} - s_{\mathrm{since}}$.

A caveat here is that reverse flow involves driving liquid towards much less mobile foam, which physically could lead to viscous fingering instabilities [13,54–57] that can arise as follows. Suppose that a high-mobility region displaces a low mobility one, and that at a certain point, the high-mobility region runs slightly ahead of the remainder of the front separating the two regions. By having a flow path that now involves slightly more high-mobility fluid and slightly less low-mobility fluid, viscous resistance is reduced, and so locally, points continue running ahead. Thus, a finger can grow. This mechanism assumes, however, that resistance is distributed over the full length of the domains extending either side of the front.

This effect is not captured by the pressure-driven growth model, which makes a different assumption regarding how resistances are distributed [29]. Resistances are taken to arise solely from low-mobility foam in what are assumed to be thin regions neighbouring the foam front. However, the front position alone is assumed to fix the extent of these thin regions. If liquid now drives a low-mobility foam front ahead of it, a region of very low-mobility foam is assumed to develop immediately behind the front. According to pressure-driven growth, displacing the front causes the extent of this region to grow, which means that resistance increases overall, tending to suppress fingering [58–60]. In effect, a limitation of the pressure-driven growth model is that it makes an implicit assumption that viscous fingering is absent [29]. That said, even for the pressure-driven growth model, there are still circumstances in which fingers can develop and subsequently grow (e.g. due to channelling owing to spatially varying permeability [42,44], see also §5g). It is purely viscous fingering [54] that is not captured.

(d) Propagation of a discontinuity

There is yet another complication which equation (3.4) considers. The effects already described, namely, dimensionless driving pressures and dimensionless resistances to flow, strictly speaking only give the velocity of the overall fluid (liquid plus foamed gas taken together). The propagation velocity of the discontinuity (i.e. of the foam front) is proportional to fluid velocity but not equal to it. It is, however, the discontinuity, rather than the overall fluid, which we aim to track.

To find how a discontinuity propagates, conservation equations are used: it is necessary to know the ratio between the jump in liquid flux and jump in liquid saturation across it [61]. Liquid flux, however, can be expressed as the product of overall fluid flux and a so-called liquid fractional flow f_l [48], with f_l being a known function of liquid saturation S_l. Thus, in the dimensionless system studied here, what is relevant for determining the velocity of a discontinuity is the ratio between the jump in fractional flow Δf_l and the jump in liquid saturation ΔS_l.

What typically happens in systems with foamed gas (both in forward flow and in reverse flow, see electronic supplementary material, fig. S1a–b in the appendix), is that jumps in fractional flow Δf_l exceed jumps in liquid saturation ΔS_l [29,38], implying then a discontinuity that propagates rather faster than an overall fluid velocity. However, if reverse flow is compared with forward flow, typically the jump in saturation ΔS_l is smaller in reverse flow. Thus, $\Delta f_l/\Delta S_l$ tends to be larger in reverse flow than in forward flow. The term $(\Delta f_l/\Delta S_l)_{\mathrm{rev/fwd}}$ appearing in equation (3.4) is the ratio between $\Delta f_l/\Delta S_l$ values in reverse and forward flow. The reason that forward flow parameters affect equation (3.4) (even though it is nominally a reverse flow equation) is due to the way that the equation has been made dimensionless, based on the set of scalings that were already established for forward flow (see electronic supplementary material, section A(c) in the appendix).

In forward flow, the value of $\Delta f_l/\Delta S_l$ turns out to be fixed, regardless of how far the front displaces. In reverse flow, however, the value of $\Delta f_l/\Delta S_l$ can vary depending upon how far the front displaces [27]. This, in turn, means that $(\Delta f_l/\Delta S_l)_{\mathrm{rev/fwd}}$ can vary. To a reasonable approximation, however, (see electronic supplementary material, section F in the appendix for details) $(\Delta f_l/\Delta S_l)_{\mathrm{rev/fwd}}$ takes a constant value (which is denoted $(\Delta f_l/\Delta S_l)_{\mathrm{rev},0/\mathrm{fwd}}$) provided $s_{\mathrm{since}} \leq s_{\mathrm{switch}}$. It then takes another constant value (which is denoted $(\Delta f_l/\Delta S_l)_{\mathrm{rev},\infty/\mathrm{fwd}}$) provided $s_{\mathrm{since}} > s_{\mathrm{switch}}$ [27]. As table 1 shows (see electronic supplementary material, table S1 in the appendix for details), $(\Delta f_l/\Delta S_l)_{\mathrm{rev},\infty/\mathrm{fwd}}$ is rather smaller than $(\Delta f_l/\Delta S_l)_{\mathrm{rev},0/\mathrm{fwd}}$. Note that the case $s_{\mathrm{since}} > s_{\mathrm{switch}}$ corresponds to a front which has propagated farther in reverse flow than in forward flow. As will be seen, this situation can actually happen. However, it only happens to some points on the front undergoing reverse flow; not all points undergoing reverse flow.

Once $s_{\mathrm{since}} > s_{\mathrm{switch}}$, as well as there being changes in the value of $\Delta f_l/\Delta S_l$ or analogously $(\Delta f_l/\Delta S_l)_{\mathrm{rev/fwd}}$, yet another change also occurs here. Specifically within the denominator of equation (3.4), one of the terms now vanishes. The low mobility region downstream of the front has now been entirely consumed, so the only resistance is from the region upstream. Physically, this implies that finely textured, low-mobility foam upstream of the front is being driven into an

almost entirely gas filled region [27,28], rather than driven into finely textured, low-mobility foam with just slightly different saturation downstream and upstream.

To summarize, the equations that must be solved are for $s_{\text{since}} \leq s_{\text{switch}}$:

$$\frac{\mathrm{d}\boldsymbol{X}}{\mathrm{d}\tau} = \frac{|Y - Y_{\text{neut}}|}{((s_{\text{switch}} - s_{\text{since}}) + M_{\text{fwd/rev}}\, s_{\text{since}})} \left(\frac{\Delta f_l}{\Delta S_l}\right)_{\text{rev},0/\text{fwd}} \boldsymbol{n}, \tag{3.6}$$

and for $s_{\text{since}} > s_{\text{switch}}$,

$$\frac{\mathrm{d}\boldsymbol{X}}{\mathrm{d}\tau} = \frac{|Y - Y_{\text{neut}}|}{s_{\text{since}} M_{\text{fwd/rev}}} \left(\frac{\Delta f_l}{\Delta S_l}\right)_{\text{rev},\infty/\text{fwd}} \boldsymbol{n}. \tag{3.7}$$

4. Analysing the pressure-driven growth model

We have solved equations (3.1)–(3.7) numerically, using a numerical scheme described in electronic supplementary material, section B (in the appendix). Before presenting numerical results (in §5), it is interesting to analyse predictions from these equations more general terms. This is done in §§ 4a–c to follow. Specifically, §4a argues that in two-dimensional systems, fronts will not simply retrace paths taken during forward flow. Then §4b considers how front speeds evolve at various stages during reverse flow. Finally, §4c discusses a point which instantaneously has moved during reverse flow the same distance as it moved during forward flow.

(a) Failure to retrace paths

In a one-dimensional system [27], a reverse flow must always retrace the same positions as it took during an original forward flow, albeit not necessarily at the same speed. In view of that, an interesting question in two-dimensional systems (as sketched in figure 1) is whether the front in reverse flow might again simply retrace the path that it took during the original forward flow. However, this is *not* the case, as can be deduced from equations (3.1) to (3.4). For any individual point that is on the front, the driving pressure difference in equation (3.4) for reverse flow (i.e. $|Y - Y_{\text{neut}}|$ in the dimensionless system) is not the same as the pressure difference Y for forward flow in equation (3.1). The resistance to flow that is presented in reverse flow, namely, $(\max(s_{\text{switch}} - s_{\text{since}}, 0) + s_{\text{since}}\, M_{\text{fwd/rev}})$ is also not the same as in forward flow, namely, s. Furthermore, the factor $(\Delta f_l/\Delta S_l)_{\text{rev/fwd}}$ (measuring the front speed relative to fluid speed) need not be the same at all points along a reverse flow front (see equations (3.6)–(3.7)).

As a consequence, it is not only the case that reverse flow causes any individual point on the front to move at different speed from what it had during an original forward flow. Instead, reverse flow also implies a quite different ratio between the speed of a given point on the front and the speed of neighbouring points on the front that are adjacent to it. This causes the front normal $\boldsymbol{n}$ to reorient during reverse flow, precluding the possibility of retracing a path that was followed during forward flow.

Indeed, it is for the very reason that points on the front do not retrace their steps, that there is a possibility as per equation (3.7) that some points might travel backwards farther than they moved forward originally. For example, if a point in forward flow starts off quite close to $Y = 0$ and then moves to the right and downwards as figure 1a shows, clearly it cannot move very far at all before motion must then cease according to equation (3.1). Once reverse flow begins, however, equations (3.6)–(3.7) could predict the point migrating all the way up to $Y = Y_{\text{neut}}$, which is farther than it moved forward originally.

A rather different case would be a point which starts off close to $Y = 1$, say, and then based on equation (3.1) moves quite some distance to the right and downwards. If it happened to reach a location just very slightly below Y_{neut} followed by the onset of reverse flow, according to equation

(3.6) it would thereafter barely move. There would now be no possibility of the distance travelled in reverse flow attaining the same value as the distance travelled in forward flow.

(b) Comparing front speeds

The analysis just presented concerned specific cases in which the value of Y (in the numerator of equation (3.1) for forward flow) is very different in magnitude from the value of $|Y - Y_{\text{neut}}|$ (in the numerator of equations (3.6)–(3.7) for reverse flow). Under these circumstances, it is obvious that these equations predict very different speeds and also very different distances displaced. A more subtle case to analyse is the one in which Y is neither very close to zero, nor very close to Y_{neut}, meaning that values of Y and $|Y_{\text{neut}} - Y|$ are comparable. In that particular situation, equation (3.1) or indeed equation (3.3) can still predict very different speeds from those predicted by equations (3.6) to (3.7). However, the differences arise now from other terms in the equations (not from those terms in Y or $|Y - Y_{\text{neut}}|$ in the respective numerators).

For instance, at the switching time τ_{switch} when reverse flow begins, the denominator in equation (3.6) is essentially s_{switch} (because s_{since} is still negligible). Moreover, s_{switch} inherits the value s which the denominator of equation (3.1) had immediately before time τ_{switch}. The implication is then that the front begins flowing faster in reverse than it had been moving in forward flow, which follows because $(\Delta f_l/\Delta S_l)_{\text{rev},0/\text{fwd}}$ in equation (3.6) is a value significantly larger than unity (see table 1). This does not, however, necessarily mean that foamed gas itself is moving faster than before, and indeed conservation laws for amounts of gas and liquid are still respected by the computations used to obtain the value of $(\Delta f_l/\Delta S_l)_{\text{rev},0/\text{fwd}}$ or indeed $(\Delta f_l/\Delta S_l)_{\text{rev/fwd}}$ more generally [27]. In forward flow, the front separates a region containing a mixture of liquid and foamed gas from a region containing only pure liquid. As §3d explains, however, the reverse flow front can separate instead regions containing only slightly different liquid saturations. What is tracked is just the location of the discontinuity. Thus the reverse flow front does not sweep all available gas before it. Instead, there is a mixture of liquid and foamed gas on both sides of the front, but with a higher proportion of foamed gas on the downstream side. Sweep in reverse is not therefore as efficient as sweep during forward flow. This then indicates another limitation of the pressure-driven growth model: the model makes it possible to compute area swept by the foam front, but that is only a surrogate measurement of how much gas is present. To determine the total amount of gas definitively, extra information would be needed regarding how liquid and gas saturations are distributed throughout the medium.

Despite the reverse flow front starting with a high speed, this high speed is not sustained. Given that $M_{\text{fwd/rev}}$ is rather larger than unity (see table 1), the front does not need to move far at all before the term $M_{\text{fwd/rev}}\, s_{\text{since}}$ in the denominator of equation (3.6) starts to become significant, and this slows the front. If a point on the reverse flow front manages to travel a distance s_{since} that approaches s_{switch}, then the front speed reaches a level that is a comparable order of magnitude to how fast the front was moving immediately before τ_{switch}. This follows because the front speed obtained from equation (3.6) now involves a ratio between two large factors $(\Delta f_l/\Delta S_l)_{\text{rev},0/\text{fwd}}$ and $M_{\text{fwd/rev}}$.

If s_{since} ever exceeds s_{switch}, however, then equation (3.7) starts to apply. A substantial fall is then seen in how fast the front is moving since, according to table 1, $(\Delta f_l/\Delta S_l)_{\text{rev},\infty/\text{fwd}}$ is much smaller than $(\Delta f_l/\Delta S_l)_{\text{rev},0/\text{fwd}}$. The implication is that a point on the front is now moving much slower than it was moving immediately before τ_{switch}. The large parameter $M_{\text{fwd/rev}}$ in the denominator of equation (3.7) also indicates that motion must be slow.

(c) Backtrack point

At any particular instant, it might be possible to identify a specific location on a reverse flow front which satisfies $s_{\text{since}} = s_{\text{switch}}$, i.e. a location corresponding to a material point which has backtracked the same distance during reverse flow as it moved originally during forward flow. This will be called the 'backtrack point'. It will be denoted $\boldsymbol{X}_{\text{back}} \equiv (X_{\text{back}}, Y_{\text{back}})$. The reverse flow

front here is considered to be made up of a collection of material points (see §3), with each material point satisfying an equation of motion, either equation (3.6) or (3.7). However, the trajectory of the backtrack point does not itself satisfy those equations. This is because the backtrack point migrates along the front from material point to material point.

This is explained as follows. Shortly after flow reversal begins, the value of s_{since} tends to be low all the way along the reverse flow front. In this case to satisfy $s_{\text{since}} = s_{\text{switch}}$, the backtrack point needs to select a material point with a low value of s_{switch}, i.e. a material point that moved comparatively little during forward flow. As already mentioned, this would correspond to selecting a material point which at the start of the forward flow was just slightly above $Y = 0$. As flow reversal proceeds, however, the value of s_{since} will grow via equation (3.5). To satisfy $s_{\text{since}} = s_{\text{switch}}$, it should now be possible for the backtrack point to select a different material point with a somewhat larger value of s_{switch}, corresponding to being somewhat higher up at the start of the forward flow. There is no requirement though for the backtrack point to travel the entire length of the reverse flow front. Indeed, as will be seen later on, there might be material points on the reverse flow front for which s_{since} never attains the same value s_{switch}, and thus the backtrack point can never reach such points.

The existence of a backtrack point implies that it is possible to have two material points which at one instant are very closely spaced, but then separate over time. This follows because on one side of the backtrack point, equation (3.6) is satisfied whereas on the other side, equation (3.7) applies. As §4b explains, these predict very different velocities. This turns out to be problematic for a numerical scheme which discretizes the front into a collection of material points. Hence, rather than having a discontinuous transition between equations (3.6) and (3.7), instead, we allow $(\Delta f_l/\Delta S_l)_{\text{rev/fwd}}$ to change continuously between $(\Delta f_l/\Delta S_l)_{\text{rev},0/\text{fwd}}$ and $(\Delta f_l/\Delta S_l)_{\text{rev},\infty/\text{fwd}}$ over a small interval of s_{since} values close to s_{switch}. We choose the interval to be 0.001 units (the same value as selected for s_0 mentioned in §§ 3a–b). Further discussion of this particular issue can be found in electronic supplementary material, section F in the appendix.

5. Results

Having explained in general terms how pressure-driven growth is expected to behave in forward and reverse flow, we now consider numerical results (obtained via the numerical scheme in electronic supplementary material, section B in the appendix). In what follows, §5a examines foam front profiles, whereas §5b considers trajectories of material points on the front. After that §5c looks at both the bottommost point on the front and the so-called backtrack point (defined as per §4c). Then, §5d explores areas swept by the foam front. Model parameters (the neutral location and also the switching time at which flow reversal onsets) are varied in §§ 5e–f. Finally, §5g looks at the effect of perturbing front shapes.

(a) Foam front profiles in forward and reverse flow

In figure 2, the foam front in forward flow is shown computed at dimensionless time $\tau = 8$ and also at $\tau = 2$. In the case $\tau = 8$, the front shape already agrees well with an approximate long-time asymptotic front shape [38] (see also electronic supplementary material, section C in the appendix for details of how this asymptotic shape can be determined). It is only close to the bottom of the front that a deviation from the long-time asymptotic shape is seen. In the case $\tau = 2$, however, the front shape has not yet converged to the long-time asymptotic shape.

Forward flow calculations like these are of course already known from literature [38]. In what follows, cases are considered in which the injection pressure is suddenly reduced (i.e. flow reversal is initiated on at least part of the front) at a time τ_{switch}, with either $\tau_{\text{switch}} = 8$ or (in subsequent sections) $\tau_{\text{switch}} = 2$ to be selected here. Thus, the front shapes shown here in figure 2 correspond to shapes at the initiation of flow reversal. What the front shapes look like after time τ_{switch} is considered in §§ 5a(i)–a(ii) below.

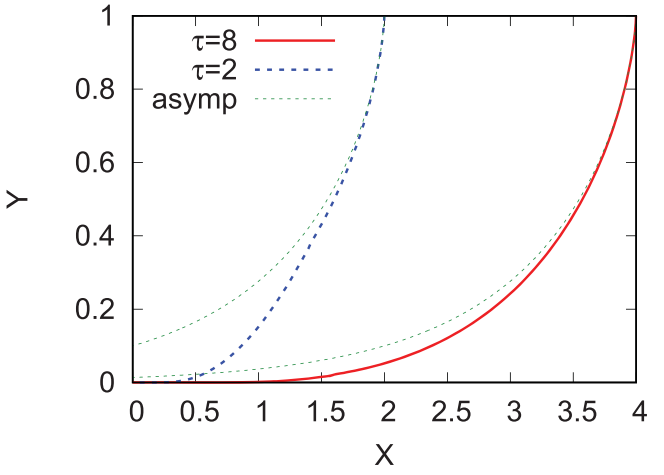

Figure 2. Foam front shapes in forward flow at dimensionless time $\tau = 8$ and also earlier on at $\tau = 2$. An asymptotic approximation to the front shape, valid at long times, is also shown.

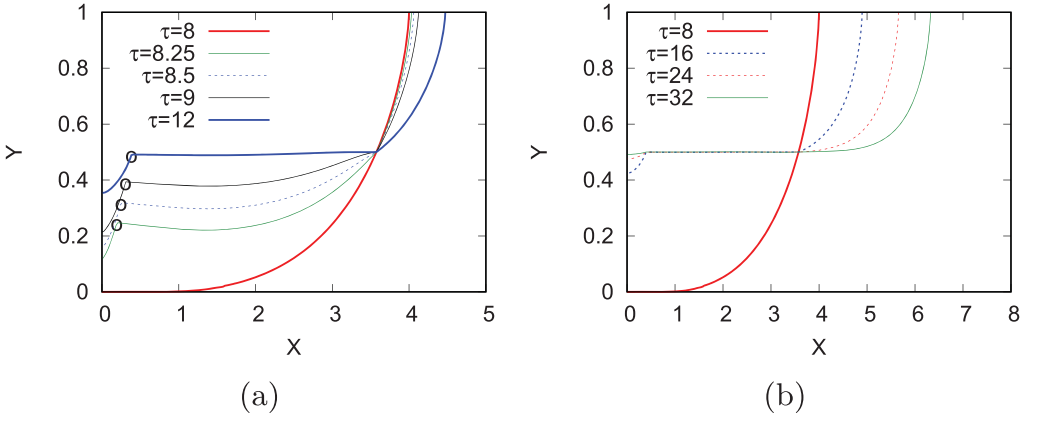

Figure 3. Foam front shapes for various times τ at or after pressure reduction in the case $\tau_{switch} = 8$ and $Y_{neut} = 0.5$ (a) up to $\tau = 12$ (b) at even longer times up to $\tau = 32$. In the case of (a), positions of the backtrack point are indicated by circles.

(i) Foam front profiles including forward and reverse flow

In figure 3a, the foam front is shown at various times τ (up to $\tau = 12$) in the case with switching time $\tau_{switch} = 8$ and neutral location $Y_{neut} = 0.5$. Remember from §3b that this specific Y_{neut} value corresponds to halving the driving pressure (i.e. halving the difference between injection pressure and the pressure within a geological porous medium). The first observation made is that (as §4b predicts), immediately after τ_{switch}, points below the neutral location move much faster than points above it. Indeed at times $\tau = 8.25, 8.5$ and 9, points above the neutral location have only moved by small amounts relative to their position at $\tau = \tau_{switch}$. Points below the neutral location have moved substantially by those same times. That said (again in line with what §4b predicts), there is also a noticeable slow down for points below the neutral location even within this time domain, e.g. the distance displaced between times 8 and 8.25 is far greater than the distance displaced between times 8.5 and 9.

It is only at approximately time $\tau = 12$ that, in the interval following the switching time $\tau_{switch} = 8$, points above the neutral location have displaced by comparable distances as those below the neutral location. Admittedly, the aspect ratio of the figure makes this slightly difficult to see, but it is easy to verify that the very top of the front has displaced approximately half a

distance unit sideways between $\tau_{\text{switch}} = 8$ and $\tau = 12$, whereas points below the neutral location have displaced approximately half a distance unit upwards. Indeed by time $\tau = 12$ much of the reverse flow front has already converged towards $Y = Y_{\text{neut}} = 0.5$ after which it can displace no farther.

Note also that starting from time τ_{switch}, a point located exactly at $Y = Y_{\text{neut}}$ ceases to move at all, as §3b mentions. Consequently, there is a point $(X_{\text{neut}}, Y_{\text{neut}})$, which for these data at least satisfies $Y_{\text{neut}} = 0.5$ and $X_{\text{neut}} \approx 3.57$, that ceases to move. This will be called the neutral point.[1] Thus, the front profiles at all subsequent times pass through this particular point.

In addition, points that are near the bottom of the front and close to the Y axis move much more slowly than other points, even to the extent of the reverse flow front appearing to develop a kink between slower moving points and faster moving ones. The slower moving points are those that barely moved forward at all during the initial forward flow, meaning they have small values of s_{switch}. It is then quite easy for s_{since} to exceed s_{switch}. The implication, as discussed in §4b, is that equation (3.7) is used, with the value $(\Delta f_l/\Delta S_l)_{\text{rev},\infty/\text{fwd}}$ being comparatively modest. This equation applies instead of equation (3.6) with a substantially larger value $(\Delta f_l/\Delta S_l)_{\text{rev},0/\text{fwd}}$ (see table 1).

Note that even though the reverse flow front is concave (as seen from downstream), and even though pressure-driven growth can potentially lead to such a front focusing into sharp concave corners [38] (see §2b), such corners tend not to develop here.[2] Evidently, the radius of curvature of the concave front at time $\tau = \tau_{\text{switch}}$ is sufficiently large, and the distance that the front displaces to reach Y_{neut} is sufficiently modest, to prevent concave corners from forming. Moreover, the kink referred to above is a convex kink, not a concave one.

One interesting feature of figure 3a is that between the convex kink and the point through which all curves pass $(X_{\text{neut}}, Y_{\text{neut}})$, the various curves at times $\tau = 8.25, 8.5$ and 9 have local minima in Y, albeit quite shallow local minima. Points close to the local minima have larger values of s_{switch} than points farther to the left (i.e. than points closer to the kink), which is why they move a bit more slowly according to equation (3.6). On the other hand, points close to the local minima start off at time τ_{switch} at Y values much smaller than points farther to the right. Moving sufficiently far to the right for example, the point $X = X_{\text{neut}}$ is reached, which by definition for all times $\tau \geq \tau_{\text{switch}}$ is located at $Y = Y_{\text{neut}}$, so it must be higher up. Having a local minimum appearing in figure 3a relies thereby on finding points with large enough s_{switch} (to avoid having quite such a rapid motion) but simultaneously starting off with quite small Y.

(ii) Parts of the front still moving forwards

Now we return to consider parts of the front with $Y > Y_{\text{neut}}$ instead of $Y < Y_{\text{neut}}$. Data are shown in figure 3b for various τ values from $\tau = \tau_{\text{switch}} = 8$ to $\tau = 32$. At $\tau = 32$, the top of the front has not even doubled the distance that it displaced by $\tau = 8$. Partly, this is due to the front presenting more resistance at later times, as represented by the s value in the denominator of equation (3.3). In addition, it is due also to the net driving pressure (the difference between injection pressure and hydrostatic pressure) being lower after time τ_{switch}. This is represented by the $Y - Y_{\text{neut}}$ factor in the numerator of equation (3.3).

In figure 4, some of the front shapes are replotted at various times included in figure 3b, but now comparing the shapes with long-time asymptotic formulae applicable for the region above Y_{neut}. These long-time asymptotic formulae are described within electronic supplementary material, section C in the appendix. In the region of interest (above and to the right of the neutral point) agreement at time $\tau = 12$ with the long-time asymptotic formula is not so good. At time $\tau = 16$, agreement is rather better. Cases with $\tau = 24$ and $\tau = 32$ are not plotted here as they cannot be distinguished from the long-time formula on the scale of the plot.

[1] By contrast, the term neutral location is intended to refer just to the vertical coordinate Y_{neut}.

[2] An exception occurs exactly on the Y-axis where a corner does in fact develop. This comes about, however, owing to a mirror symmetry condition, as mentioned in §3b.

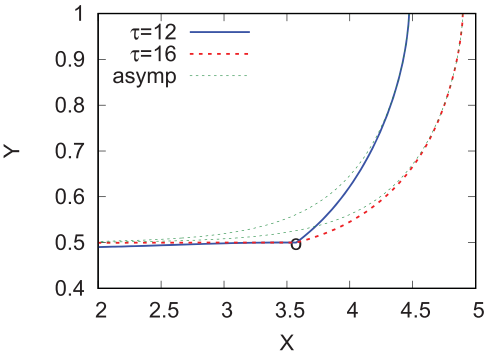

Figure 4. Foam front shapes at $\tau = 12$ and $\tau = 16$ (for $\tau_{switch} = 8$ and $Y_{neut} = 0.5$) compared with long-time asymptotic formulae in the region above the neutral location Y_{neut}. The neutral point (X_{neut}, Y_{neut}) is marked as a circle.

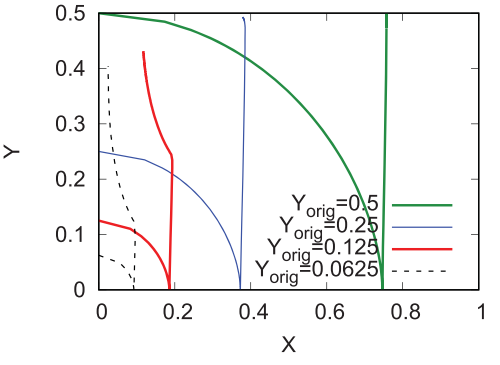

Figure 5. Trajectories followed by material points originally at various locations Y_{orig} on the Y-axis, specifically for the values $Y_{orig} = 0.0625, 0.125, 0.25$ and 0.5. These data have switching time $\tau_{switch} = 8$ and neutral location $Y_{neut} = 0.5$, and points are followed up to a final time of 16. Starting from the Y-axis, material points first move to the right and downward. After that, they move almost vertically upwards. In some cases, they then move leftwards as well as upwards.

Considering the $\tau = 16$ case again, it is remarkable that agreement is so good given that the top of the front has advanced horizontally only approximately one distance unit from the neutral point (X_{neut}, Y_{neut}). In figure 2 by contrast, which compared the front shape with an asymptotic formula from the literature [38] applicable prior to reduction in injection pressure, it was necessary to advance as many as four distance units to obtain reasonable agreement. The analysis in section C, however, makes it clear that after a reduction in injection pressure, convergence to the long-time formulae should occur over smaller distances, and figure 4 verifies this.

Once the front shape in what is now called the upper region (above the neutral location) has converged to a long-time formula, it is very straightforward to predict subsequent system behaviour. In what follows, therefore, we return to focus on what is now called the lower region (below the neutral location) which is more challenging to understand.

(b) Trajectories of selected material points

Further insights can be obtained by plotting in figure 5, the (X, Y) trajectories over time of selected material points on the front (as opposed to the (X, Y) shape of the whole front at selected times). All points start at $X = 0$ but at different Y. We start by considering the point originally at $Y_{orig} = 0.125$. This starts off moving primarily horizontally early on, but the direction of motion also gradually develops a downwards vertical component. The point approaches the bottom boundary $Y = 0$ after which it effectively stops moving, at least up until the switching time

$\tau_{\text{switch}} = 8$. The location at which it stops moving turns out to be at $X \approx 0.186$. To reach the bottom boundary, the point has displaced farther in the horizontal than in the vertical, by a factor of approximately 1.5.

Immediately after time τ_{switch}, it is clear from figure 5 that motion of the material point (still for the case $Y_{\text{orig}} = 0.125$) is primarily vertical. However, after moving upwards a certain height, which is approximately twice the value of Y_{orig}, it develops a velocity component to the left as well as upwards. This corresponds to the kink in figure 3a reaching and then passing through the material point in question. As long as a material point is still to the right of the kink in figure 3a but below the neutral location, the point normal is directed primarily upward. However, if the kink in figure 3a displaces over time such that the material point is to the left of the kink, the point normal is directed both upward and leftward. Moreover, once the point is to the left of the kink, the motion is also quite slow. As a result, by the final time considered in figure 5 (which is $\tau = 16$), the point that is currently being discussed (with $Y_{\text{orig}} = 0.125$) is still some distance away from the neutral location $Y_{\text{neut}} = 0.5$.

A similar pattern is seen for a material point that starts lower down at $Y_{\text{orig}} = 0.0625$ although Y now approaches zero at a proportionally smaller X value ($X \approx 0.092$). The X displacement still, however, exceeds the Y displacement, again approximately by a factor 1.5. After time τ_{switch}, near vertical motion proceeds again up to approximately twice Y_{orig} (albeit Y_{orig} is now smaller than before). After that motion is both upward and leftward.

Considering now a material point with $Y_{\text{orig}} = 0.25$, behaviour is yet again similar. During the initial forward flow, the value of Y approaches zero for $X \approx 0.372$, and stays at that location until time τ_{switch}. After time τ_{switch} there is near vertical motion, albeit with a slight rightward drift. This rightward drift is associated with the curves in figure 3a having local minima in Y for intermediate X values, such that some of the normals point slightly to the right. The near vertical motion now proceeds almost all the way up to $Y_{\text{neut}} = 0.5$. The curve then deviates towards the left, though this is difficult to see in figure 5, as the deviation occurs only when the curve is already very close to $Y_{\text{neut}} = 0.5$. This is again consistent with deviating to the left only when Y is approximately twice Y_{orig}, but with twice Y_{orig} now equalling $Y_{\text{neut}} = 0.5$. The kink in figure 3a evidently does manage to catch up with this material particular point, but only barely manages to do so.

Finally, a material point is considered with $Y_{\text{orig}} = 0.5$. During forward flow, Y only approaches zero only around location $X \approx 0.746$, and stays there until time τ_{switch}. After time τ_{switch}, the material point moves upwards (again with a very slight rightward drift). In this case, however, there is no sudden deviation towards the left. This now implies an X value sufficiently large that the kink in figure 3a never manages to catch it.

(c) Bottom of the front and backtrack point

In what follows, we consider the evolution of the bottommost point of the front (§5c(i)) and then the backtrack point is considered (§5c(ii)–c(iii)).

(i) Bottom of the front

In figure 6, the bottommost point of the front Y_{bot} is plotted as a function of time τ. This point is always at $Y = 0$ up until $\tau_{\text{switch}} = 8$. After that it moves upward, approaching $Y_{\text{neut}} = 0.5$ at very long times. However, the rate of approach of Y_{bot} to Y_{neut} is very slow. Even after 30 time units, it is still possible to see a difference between Y_{bot} and Y_{neut} in figure 6.

Starting from equation (3.7), it is possible to derive an analytical formula for Y_{bot} (see electronic supplementary material, section D in the appendix). This formula, is however, in implicit form (i.e. time τ as a function Y_{bot}), so is a little awkward to use. It is not plotted in figure 6 because it would be indistinguishable from the numerical data already shown. Rather more useful, however, is a long-time asymptotic approximation to Y_{bot} (see electronic supplementary material, equation (D.4), which is in explicit form); this is plotted on figure 6. The explicit formula (see

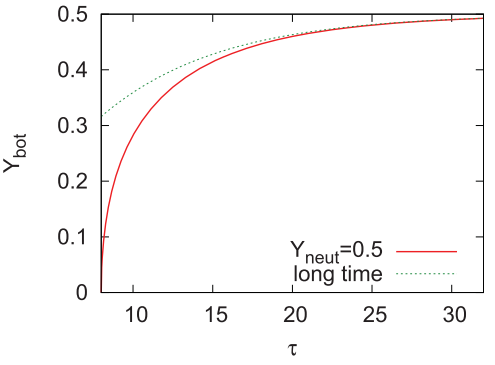

Figure 6. Position of the bottom of the front Y_{bot} versus time τ for $\tau_{\text{switch}} = 8$ and $Y_{\text{neut}} = 0.5$.

electronic supplementary material, equation (D.4)) makes it clear that the typical time scale for Y_{bot} to approach Y_{neut} is $Y_{\text{neut}} M_{\text{fwd/rev}} (\Delta f_l / \Delta S_l)^{-1}_{\text{rev},\infty/\text{fwd}}$, where $Y_{\text{neut}} = 0.5$ here, while values of $M_{\text{fwd/rev}}$ and $(\Delta f_l / \Delta S_l)_{\text{rev},\infty/\text{fwd}}$ are listed in table 1. This turns out to imply quite a long-time scale because $M_{\text{fwd/rev}}$ in particular is significantly larger than unity.

(ii) Locus of backtrack point

The next quantity to be examined is the so-called backtrack point $\boldsymbol{X}_{\text{back}} \equiv (X_{\text{back}}, Y_{\text{back}})$. This is calculated (see §4c) as the point at which instantaneously $s_{\text{since}} = s_{\text{switch}}$, i.e. the point has backtracked by the same distance that it moved forward initially. This means that the speed suddenly falls, by changing from equations (3.6) to (3.7), remembering here that $(\Delta f_l / \Delta S_l)_{\text{rev},0/\text{fwd}}$ in equation (3.6) is significantly larger than $(\Delta f_l / \Delta S_l)_{\text{rev},\infty/\text{fwd}}$ in equation (3.7). It follows that the kink in figure 3a should correspond to the backtrack point. We have verified that this is the case within figure 3a, by the simple procedure of superposing backtrack point positions on top of front shapes.

Figure 7a plots the locus of the backtrack point. The main observation from figure 7a is that this is very close to a straight line. The next observation is that Y_{back} is just a little larger than X_{back}. That this should be the case makes geometric sense. Initially, at time $\tau = 0$, the foam front lies along the Y-axis. This means that, during forward flow, points forming the front initially move horizontally, but eventually (as the front reorients) they must also acquire a vertical velocity component downwards. However, the horizontal displacement during forward flow remains greater than the vertical displacement, as figure 5 clearly indicates. By time τ_{switch}, the displaced distance s_{switch} must exceed, even if only slightly, the X value reached.

At time $\tau = \tau_{\text{switch}}$, it is clear (from figure 3a) that there is a significant region along the bottom of the front which is nearly horizontal. This extends at least as far as $X = 1$. As §5b discusses in detail, after the front reverses, points on this nearly horizontal part of the front must displace almost vertically. As figure 5 shows, their Y value changes, but their X value does not. To a good approximation, therefore, the displaced distance since flow reversal then satisfies $s_{\text{since}} \approx Y$. By definition, however, the backtrack point is the point at which $s_{\text{since}} = s_{\text{switch}}$. It follows therefore that $Y_{\text{back}} \approx s_{\text{switch}}$. However, it has already been commented that s_{switch} slightly exceeds the X value that a given point reaches. Thus, Y_{back} slightly exceeds X_{back} just as figure 7a finds. Note, however, that when the backtrack point $(X_{\text{back}}, Y_{\text{back}})$ catches up with a material point at given location (X, Y), the material point in question no longer continues moving almost vertically. This has already been seen in the context of figure 5.

It is also of interest to relate the original Y location of a material point (denoted Y_{orig}) with the position that it has $(X_{\text{back}}, Y_{\text{back}})$ at the instant when the backtrack point catches it. In §5b, it was found that the horizontal displacement during forward flow is up to $X \approx 1.5\, Y_{\text{orig}}$. Then during reverse flow, points move mostly vertically (i.e. their X value does not change) until the backtrack point catches them, implying that to a reasonable approximation $X_{\text{back}} \approx 1.5\, Y_{\text{orig}}$. Section 5(b)

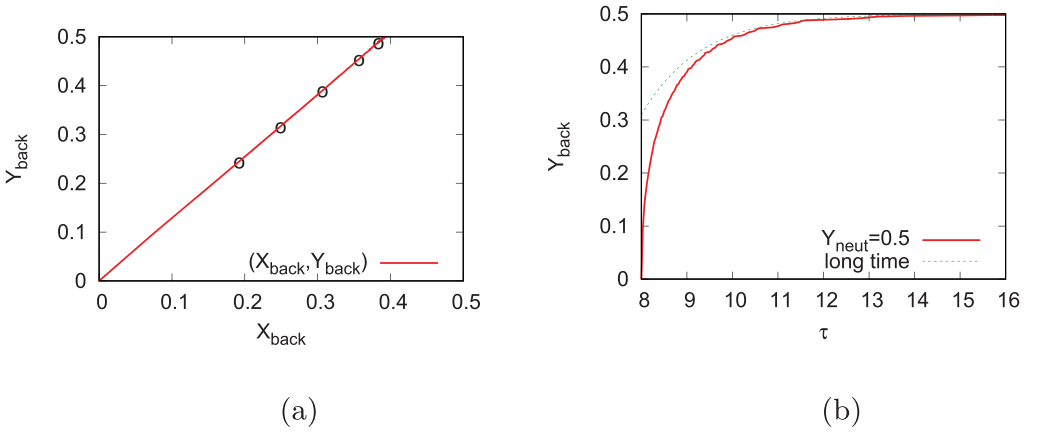

Figure 7. (a) Locus of the backtrack point (X_{back}, Y_{back}) for $\tau_{switch} = 8$ and $Y_{neut} = 0.5$. The backtrack point is at the origin at time τ_{switch}. The circles correspond to the times 8.25, 8.5, 9, 10 and 12. (b) Backtrack point vertical position Y_{back} versus time τ for $\tau_{switch} = 8$ and $Y_{neut} = 0.5$.

also found, however, that $Y_{back} \approx 2\,Y_{orig}$. It then follows that $X_{back} \approx 0.75\,Y_{back}$ which is broadly consistent with figure 7a, albeit $X_{back} \approx 0.8\,Y_{back}$ turns out to be a slightly better fit to figure 7a.

Another observation from figure 7a is that X_{back} never exceeds 0.4 whereas the value of X_{neut} (identified in §5a(i)) is more than three distance units above that. Hence in much of the domain that is below the neutral location Y_{neut}, points are already so far to the right that they can never move backwards farther than they moved forward, i.e. they never turn out to have a s_{since} value exceeding s_{switch}. Hence, over much of the reverse flow front, there is never a need to switch from equation (3.6) which evolves rather quickly to equation (3.7) which evolves slowly.

If much of the foam front is moving backwards quickly, that might seem at first sight like an indication that gas can be extracted quickly. Remember, however, (§3d and §4b) that what the front is now modelling is merely a discontinuity separating drier foam on one side from somewhat wetter foam on the other. Moving the front rapidly therefore does not imply that all available gas is swept equally rapidly ahead of it.

(iii) Time evolution of backtrack point

In figure 7b, we plot how Y_{back} evolves with time τ starting from $\tau_{switch} = 8$. Given that the locus of (X_{back}, Y_{back}) is so close to a straight line, knowing how Y_{back} evolves with time automatically implies how X_{back} evolves also. The first observation made is that the shape of Y_{back} as a function of τ is qualitatively similar to that of Y_{bot} a function of τ in figure 6. What is different, however, is the rate of evolution which is much faster in the case of Y_{back}. Already by approximately 12 time units, Y_{back} is close to Y_{neut}. The second observation, looking closely, is that the data for Y_{back} are slightly noisy. There is a numerical reason for this and also a way to remove the noise (see electronic supplementary material, section F(b) in the appendix). Here, however, in figure 7b, we decided that the noise, although present, was at a sufficiently low level that it was not essential to remove it.

It is possible also to predict (see electronic supplementary material, equation (E.3) in the appendix) how Y_{back} should evolve with time τ under the approximation (already described) that points start close to $Y = 0$ at time $\tau = \tau_{switch}$ and then move primarily vertically upwards. This produces an implicit relation (i.e. τ as a function of Y_{back}). This has not been plotted here, as it turns out to be such a good approximation that it is difficult to distinguish from the numerical predictions (aside from a small amount of noise in the numerics as already mentioned). Of interest, however, is a long-time asymptotic prediction for the evolution of Y_{back} (see electronic supplementary material, equation (E.5)). This is now an explicit equation and it is plotted on figure 7b. Electronic supplementary material, equation (E.5) makes it clear that the typical time

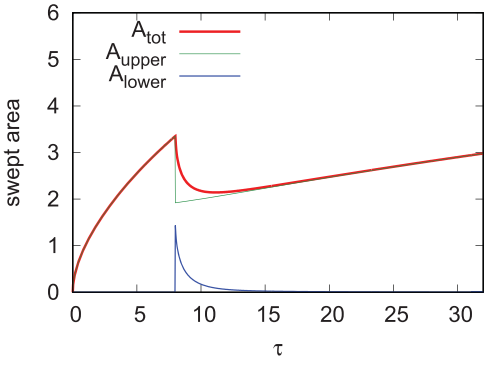

Figure 8. Swept areas A_{tot}, A_{upper} and A_{lower} versus time τ for $\tau_{\text{switch}} = 8$ and $Y_{\text{neut}} = 0.5$.

scale for Y_{back} to approach Y_{neut} is $Y_{\text{neut}} M_{\text{fwd/rev}} (\Delta f_l / \Delta S_l)^{-1}_{\text{rev},0/\text{fwd}}$. Even though $M_{\text{fwd/rev}}$ is itself quite large, the comparatively large value of $(\Delta f_l / \Delta S_l)_{\text{rev},0/\text{fwd}}$ (see table 1) is what keeps this time scale much smaller than the analogous time scale for Y_{bot} (see §5c(i)).

(d) Swept areas

Areas that have been swept by the front as a function of time are plotted in figure 8. Swept areas (computed at any instant as $\int X \, \mathrm{d}Y$ via quadrature) give some indication of the amount of gas that is present in the system, although not full information about this. As already alluded to (see §3d and §4b), the foam front merely indicates positions in which there is a discontinuous jump in liquid saturation. The swept area would only match the amount of gas present in a hypothetical case in which the discontinuous jump in saturation was from zero to unity, which is certainly not the case (see electronic supplementary material, table S1 in the appendix for details). To determine the actual amount of gas present, it would be necessary to know (again see §4b) gas saturation at all positions in the system, including positions away from the front which pressure-driven growth does not interrogate.

In figure 8, three types of swept area have been identified: a total swept area A_{tot}, an upper swept area A_{upper} (pertaining to the part of the front that is moving forwards) and a lower swept area A_{lower} (pertaining to the part of the front that is in reverse flow). Prior to the switching time $\tau_{\text{switch}} = 8$, all points on the front are moving forwards, so by definition A_{upper} equals A_{tot}, whereas A_{lower} vanishes. At time τ_{switch}, however, there is a non-zero A_{lower} (corresponding now to swept area below the neutral location), and so A_{upper} (swept area above the neutral location) must also change to compensate. Moving just beyond time τ_{switch} though, A_{lower} decays rapidly, and as a result A_{tot} also exhibits rapid decay. In addition, A_{upper} grows but more slowly. By approximately time $\tau = 12$ most of the lower area has disappeared, so A_{tot} is now very close to A_{upper}, and is growing with time. Growth is sufficiently slow, however, that by time $\tau = 32$, the swept area A_{tot} has still not recovered the same value as it had at time $\tau = \tau_{\text{switch}}$.

Earlier it was found (see figure 4) that reasonably soon after time τ_{switch}, the foam front shape in the upper region (above the neutral location) tends to approach a long-time asymptotic form (see also electronic supplementary material, section C in the appendix). Once this long-time asymptotic shape is known, the area swept by it is easy to compute. Given moreover that the area in the lower region decays comparatively quickly, it follows that the total area A_{tot} should also approach this same asymptotic formula for area just for the upper region. Figure 9 verifies that this is the case.

(e) Effect of changing neutral location

Now we explore distinct values of neutral location Y_{neut}, not just $Y_{\text{neut}} = 0.5$ considered to date. Specifically, $Y_{\text{neut}} = 0.25$ and $Y_{\text{neut}} = 1$ are considered, still with switching time $\tau_{\text{switch}} = 8$. Effects upon foam front profiles (§5e(i)) and swept areas (§5e(ii)) are examined.

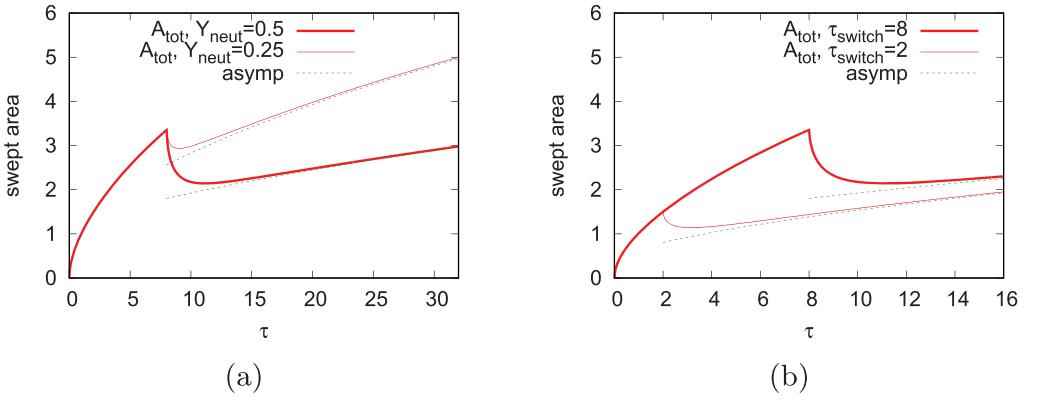

Figure 9. Swept area A_{tot} (a) for $\tau_{switch} = 8$ and either $Y_{neut} = 0.5$ or $Y_{neut} = 0.25$, (b) for $Y_{neut} = 0.5$ and either $\tau_{switch} = 8$ or $\tau_{switch} = 2$. The A_{tot} values are compared with long-time asymptotic formulae.

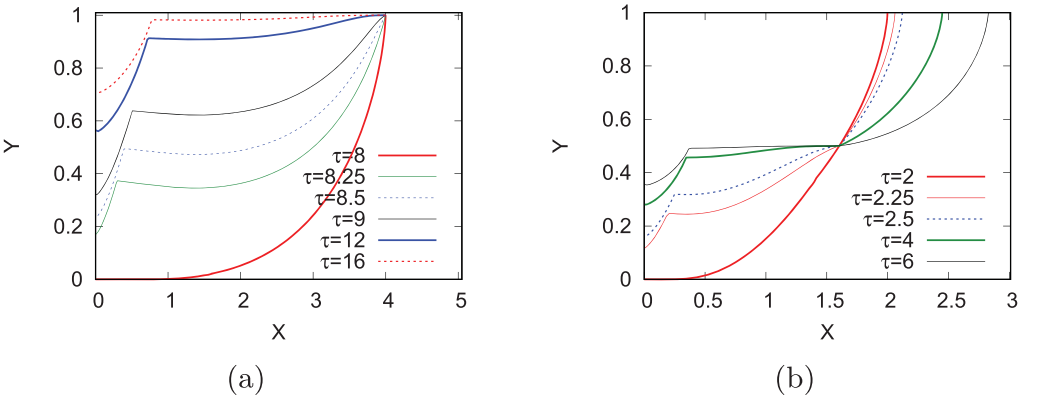

Figure 10. (a) Foam front shapes at various times τ for (a) $\tau_{switch} = 8$ and $Y_{neut} = 1$ and (b) $\tau_{switch} = 2$ and $Y_{neut} = 0.5$.

(i) Effect of neutral location upon foam front profiles

For different values of neutral location Y_{neut}, profiles of front shape (Y as a function of X) can be obtained at various times. However, in the case of $Y_{neut} = 0.25$, the profiles are qualitatively the same as that seen in figure 3, so we choose not to present them here. In short, immediately after the switching time τ_{switch}, rapid evolution is seen in most of the lower region, i.e. below the neutral location. Evolution in the upper region (i.e. above the neutral location) is slower. Moreover, a kink develops in the lower region, and to the left of that kink, evolution is very slow.

Of more interest are plots of (X, Y) profiles in the case $Y_{neut} = 1$. This corresponds to complete removal of the injection pressure. Data are plotted in figure 10a. Now there is no upper region at all, only a lower region. The evolution is still quite rapid, e.g. a kink again develops and it takes only approximately half a time unit for this kink to travel vertically half way up the domain. In relative terms, however, the evolution is slower than before (contrast with e.g. figure 3). For instance, in figure 3 at time $\tau = 12$, much of the front is already very close to $Y = Y_{neut} = 0.5$. However, in figure 10a at time $\tau = 12$, the front is still some way from $Y = Y_{neut} = 1$. Indeed, it takes until time $\tau = 16$ before much of the front is close to $Y = 1$.

Although not shown here, data for Y_{bot} and Y_{back} as functions of time τ for $Y_{neut} = 1$ also support this notion of slower evolution in relative terms. In fact (as the formulae given in

electronic supplementary material, sections D–E in the appendix suggest, see e.g. electronic supplementary material, equations (D.2) and (E.3)), data can be collapsed together with different Y_{neut} by plotting Y_{bot}/Y_{neut} as a function of $(\tau - \tau_{switch})/Y_{neut}$, and analogously by plotting Y_{back}/Y_{neut} as a function of $(\tau - \tau_{switch})/Y_{neut}$. Indeed, the reason these data are not shown here is because the curves with different Y_{neut} collapse together so well that they cannot be distinguished from one another on the scale of the plot. Hence, the shapes of the curves for different Y_{neut} can already be deduced from the curves shown in figure 6 and figure 7b. Swept areas, however, are slightly different from what has been seen before as is discussed next.

(ii) Effect of neutral location upon swept areas

If instead of selecting a neutral location $Y_{neut} = 0.5$, we now consider $Y_{neut} = 0.25$, say, swept area A_{tot} (as plotted in figure 9a) is seen to fall only by a modest amount after time τ_{switch}. After that A_{tot} starts growing again, and grows more rapidly than in the case $Y_{neut} = 0.5$. Indeed, already by $\tau = 32$, the area A_{tot} for $Y_{neut} = 0.25$ is larger than it was at time $\tau_{switch} = 8$.

Comparing the two different cases with different Y_{neut} values shown on figure 9a, it is interesting to speculate whether it might be possible to vary Y_{neut} with time to keep A_{tot} essentially fixed after time τ_{switch}. In other words, decay in A_{lower} would compensate growth in A_{upper}. That could be considered to approximate a situation in which a system is shut in [27], with no more net gas entering after time τ_{switch}: this could be relevant to sequestering a gas such as CO_2 [25]. Note that, fixing swept area is only an approximation to sequestration, as fixing area is not the same as fixing the amount of gas in a system (see §5d). Nonetheless, swept area should at least give an indication of the amount of gas. Evidently for A_{tot} to remain fixed, it would be necessary to have a very small value of Y_{neut} initially (to prevent any rapid initial fall in A_{tot} immediately after τ_{switch}). Then, it would be necessary to increase the values of Y_{neut} over time (thereby to prevent A_{tot} from rising later on). Given how Y_{neut} is defined (see §3b), this is equivalent to reducing injection pressure gradually over time.

That said, we have not carried out any time-varying Y_{neut} calculations here owing to a slight complication in implementing them. Provided the value of Y_{neut} is fixed with time, it is clear from equations (3.3) to (3.4) that a material point at the neutral location at time τ_{switch} will always remain at the neutral location thereafter, i.e. it ceases to move as §3b already mentions. Equivalently, the neutral point (X_{neut}, Y_{neut}) (see §5a(i)) is fixed. Moreover, after time τ_{switch}, any other material point away from the neutral location, will always remain either in the upper region (if above the neutral location) or in the lower region (if below it), without ever crossing the neutral location. Our current computer implementation of pressure-driven growth makes use of these features to simplify computations: in effect after time τ_{switch}, the front shapes in the upper region and the lower region can be computed independently of each other. Some reworking would be needed to generalize to a system with time-varying Y_{neut} in which these simplifying features are lost.

Figure 9a focused on total swept area A_{tot} which tends at long times to coincide with upper swept area A_{upper}, at least after the lower swept area A_{lower} has decayed. However, it is also interesting to consider the decay of A_{lower} itself and how the decay is affected by the value of Y_{neut}. This is considered in figure 11a. Obviously changing the neutral location Y_{neut} changes the relative amounts of swept area assigned as lower and upper area. However, it is possible to compensate for this by considering A_{lower} normalized say by its initial value at time τ_{switch}. In figure 11a, this normalized area is plotted (on a logarithmic scale) against $(\tau - \tau_{switch})/Y_{neut}$. The rescaling of time here is suggested by e.g. electronic supplementary material, equations (D.2) and (E.3) in the appendix.

Considering the different Y_{neut} values, good agreement is seen in figure 11a for the early time decay. However, at longer times, the $Y_{neut} = 0.25$ case decays faster than the $Y_{neut} = 0.5$ case, and the $Y_{neut} = 1$ case decays more slowly. To understand this effect at longer times, it is first recalled that there is a kink in the foam front shape (as in figure 3a), with areas to the left of the kink decaying much slower than areas to the right. Equivalently points to the left of the kink, including

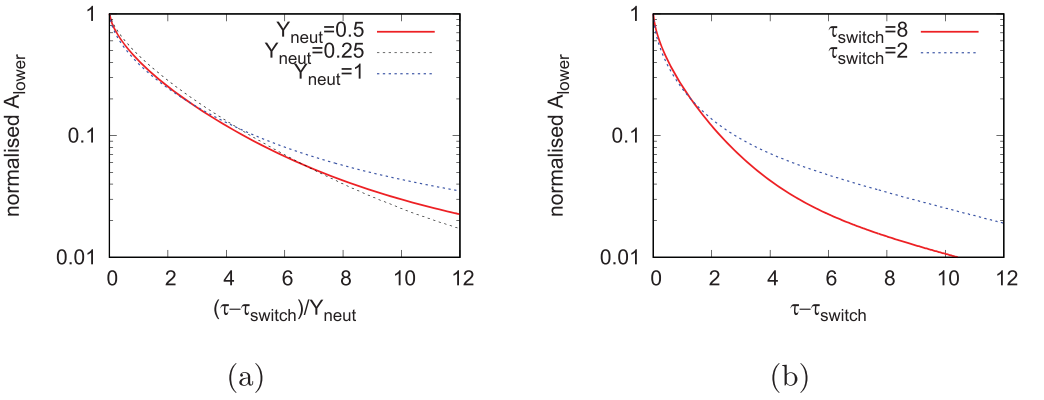

Figure 11. (a) Normalized A_{lower} versus $(\tau - \tau_{switch})/Y_{neut}$ for various Y_{neut}. Here, $\tau_{switch} = 8$. (b) Normalized A_{lower} versus $(\tau - \tau_{switch})$ for various τ_{switch}. Here, $Y_{neut} = 0.5$.

the bottommost point Y_{bot} (figure 6), reach a final state more slowly than the kink itself located at Y_{back} (figure 7b). It is by estimating these various contributions to area and how they decay, that the findings in figure 11a can be explained, as discussed below.

For a given Y_{neut}, and at a time $\tau = \tau_{switch}$ which is not too large, the lower region (below the neutral location) in figure 3a is approximately on the order of unity in horizontal extent, while the vertical extent is Y_{neut} by definition. The area scales therefore proportionally to Y_{neut}. Later on though, it is the above mentioned slowly decaying area to the left of the kink which accounts for most of what remains of the swept area A_{lower}. It is possible to argue that this slowly decaying region has an area that scales proportionally to Y_{neut}^2 (see details in electronic supplementary material, section E(b) in the appendix). In relative terms then, the ratio between the area of the slowly decaying region (order Y_{neut}^2) and the lower swept area prior to any decay (order Y_{neut}) itself scales proportionally to Y_{neut}. Thus, the slowly decaying region accounts for a higher proportion as Y_{neut} grows.

Another check which can be done (not presented here) is to normalize the areas by Y_{neut}^2 (instead of by the initial area A_{lower} at time τ_{switch}). Retaining a logarithmic scale as per figure 11a, the data can be shown to collapse at large values of $(\tau - \tau_{switch})/Y_{neut}$. As mentioned, all that survives at long times is the area to the left of the kink, which does indeed scale like Y_{neut}^2 (again see electronic supplementary material, section E(b) for the explanation of the order Y_{neut}^2 scaling).

(f) Effect of varying switching time

Now, instead of varying the neutral location Y_{neut}, the effect of varying the switching time τ_{switch} is explored. Specifically, we consider a value $\tau_{switch} = 2$ (instead of $\tau_{switch} = 8$ previously) with $Y_{neut} = 0.5$. Foam front shapes are shown in figure 10b. As the upper region will eventually approach a well characterized long-time asymptotic shape (see e.g. electronic supplementary material, section C in the appendix), the focus here is upon the lower region (below the neutral location).

Again over much of the lower region, rapid evolution is seen shortly after time τ_{switch}, albeit with convex kinks developing, and there is slow evolution to the left of a kink. Even as early as time $\tau = 6$, the front to the right of the kink has converged to the location $Y_{neut} = 0.5$. One contrast between figures 3a and 10b is that in the latter, local minima in Y are no longer seen. Owing to the smaller τ_{switch}, in figure 10b, there is a much smaller horizontal spatial separation between the kink and the neutral point. The value of Y therefore rises more sharply with X to reach (X_{neut}, Y_{neut}) now with $X_{neut} \approx 1.60$, which prevents local minima from forming.

As well as considering foam front shapes, it is also possible to look at Y_{bot} and Y_{back} as functions of time. Upon changing from $\tau_{switch} = 8$ to $\tau_{switch} = 2$, it turns out though that Y_{bot} and

Y_{back} (provided they are plotted as functions of $\tau - \tau_{\text{switch}}$) are indistinguishable from figures 6 and 7b so are not presented here. There is a slight difference in the value of X_{back}, however, as explained in electronic supplementary material, section F(c) in the appendix.

Now we turn to analysing swept areas (see figure 9b). Obviously, when $\tau_{\text{switch}} = 2$ instead of $\tau_{\text{switch}} = 8$ is selected, a decay in the total swept area A_{tot} is seen beginning earlier in τ. However, the amount that A_{tot} decays is less. This follows because the decay is associated with loss of swept area below the neutral location starting from time τ_{switch}. In figure 10a (with $\tau_{\text{switch}} = 2$), there is less area to be lost than in figure 3a (with $\tau_{\text{switch}} = 8$). At later times in figure 9b, A_{tot} begins to increase again.

It is again of interest to analyse evolution of the lower swept area A_{lower}. Specifically, in figure 11b, we plot a normalized value of A_{lower} (i.e. normalized by the value of A_{lower} at time τ_{switch}) and shown on a logarithmic scale. This is plotted against $\tau - \tau_{\text{switch}}$. Initially, the cases $\tau_{\text{switch}} = 2$ and $\tau_{\text{switch}} = 8$ are in agreement. Later on though, the normalized A_{lower} is larger when τ_{switch} is smaller. This is because, with smaller τ_{switch}, the slowly decaying area to the left of the kink (in figure 10b) represents at any given $\tau - \tau_{\text{switch}}$, a larger fraction of the initial area A_{lower} that is swept at time τ_{switch}. Although data are not presented here, it is also possible to remove the normalization by this initial A_{lower} but still plot on a logarithmic scale. This reveals that unnormalized A_{lower} values agree at long times despite having different τ_{switch}.

(g) Effect of perturbing front shape

Yet another case to be considered is one in which a perturbation has developed on the foam front shape by time τ_{switch}. This could model a heterogeneous situation in which permeability varies spatially in the medium, so that by time τ_{switch} certain parts of the front have run ahead and other parts lag behind. Thus, an oscillatory perturbation in space is superposed on the front shape. Perturbed front shapes arising from varying permeability have been studied previously in forward flow [42,44], but never in reverse flow.

Parts of the front that run ahead during forward flow, start from behind when flow reverses after time τ_{switch}. Remember though that (see §4a), during reverse flow, points do not retrace the same paths as they took during forward flow. Thus, there is no guarantee that points on the front experience, during reverse flow, the same set of varying permeabilities as may have caused a perturbation to develop during forward flow. Hence, there is no guarantee that imposing reverse flow will undo any perturbation to the front shape. Here, for simplicity, changes in permeability are not considered explicitly. Instead, we merely study the effect of adding oscillatory perturbations to the front shape at time τ_{switch}, consistent with the sort of perturbation which spatially varying permeability might produce [42,44]. In other words, what is studied here formally is a homogeneous medium, but with a spatial perturbation superposed on the front shape. The exact form of the perturbations assumed to develop by time τ_{switch} is given in electronic supplementary material, section G in the appendix. Perturbations are introduced only below the neutral location, because their effect on forward flows (above the neutral location) is already well known [42,44].

What is observed in figure 12 is that at time τ_{switch} instead of having a concave front (seen from the downstream direction) there is, owing to the perturbation, a sequence of concavities and convexities. These are in different positions in figure 12a,b, because the perturbations imposed in one figure are selected to be opposite in sign to the perturbations in the other. In both cases though at time τ_{switch}, the curvature of the concavities in particular is much sharper than in figure 3a.

As the front undergoes reverse flow and time proceeds, it is this increased curvature which allows the concavities to focus down into sharp concave corners (see e.g. §2b). Already by approximately time $\tau = 8.5$ or $\tau = 9$ some concave corners have formed, albeit again in different positions in figure 12a,b. The other observation here, in both cases figure 12a–b, is that the amplitude of the perturbation decays over time. This follows because the speed of any point on the front must fall towards zero as Y approaches the neutral location Y_{neut}. Clearly, the convex

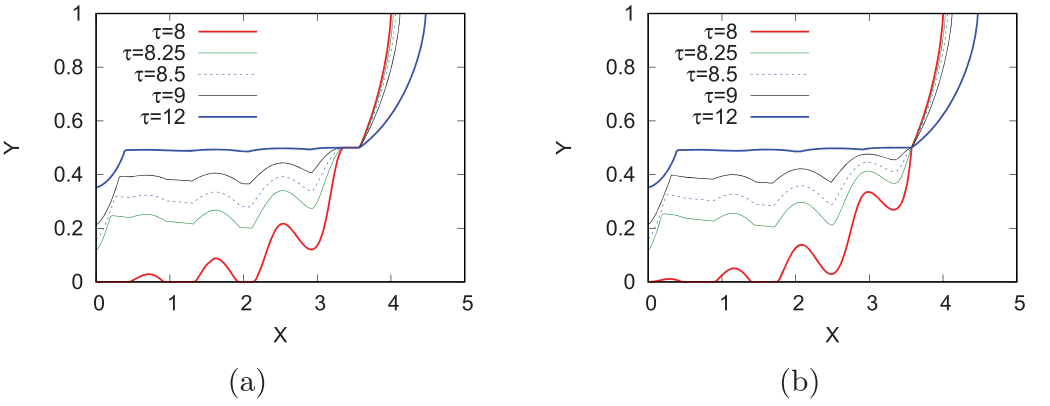

Figure 12. Evolution of front shape when a front is perturbed at time $\tau_{\text{switch}} = 8$. Here, $Y_{\text{neut}} = 0.5$. The perturbation is (a) upwards close to the neutral location and downwards close to the bottom, and (b) downwards close to the neutral location and upwards close to the bottom.

parts of the front approach Y_{neut} sooner, but then their speed falls, and the concave parts of the front catch them up. By time $\tau = 12$ much of the front has already reached Y_{neut}, apart from a slow moving region near the Y axis (to the left of a convex kink).

As well as examining front shapes, it is also possible to examine the time evolution of quantities such as Y_{bot} and Y_{back}. These turn out, however, to be indistinguishable from the unperturbed case (figures 6 and 7b), so are not plotted there. There is a slight difference in the case of X_{back} (see electronic supplementary material, section F(c) in the appendix). It is also possible to examine the time evolution of swept area A_{lower}, but again this can barely be distinguished from the unperturbed case. This, however, is unsurprising given that area is an integral quantity which averages over the upwards and downwards perturbations that are imposed here.

6. Conclusion

In conclusion, the pressure-driven growth model offers a quick and simple way to explore foam flow in porous media. Past work with the model has focused on forward-flowing foam fronts. In the present work, however, the model has been used to study propagating foam fronts for which a driving injection pressure is reduced at a certain switching time. Part of the foam front (below a so-called neutral location) is then set into reverse flow. This then could be a model for seasonal storage and subsequent extraction of an energy carrying gas. For simplicity, a homogeneous, isotropic medium has been considered, although it is also possible to extend the approach to heterogeneous, anisotropic cases.

The model indicates that the reverse flow front does not simply retrace its original path, but instead travels at different speed and also in a different direction. Some points on the reverse flow front (those near the bottom and near the vertical axis) move farther in reverse flow than in forward flow, although most points on the foam front do not achieve that. Indeed, the front stops once it reaches the neutral location.

It has also been predicted that foam fronts, upon the onset of reverse flow, move surprisingly fast, albeit they then slow down with time. This can be seen in foam front profiles themselves (barring a very small slow moving portion of the front near the bottom and the vertical axis). It is also seen in plots of the evolution of the so-called backtrack point, and in plots of the evolution of areas swept by the front.

On the other hand, points higher up on the foam front (those above the neutral location) which continue in forward flow move less quickly. Even so, they do not need to move very far at all before they attain a long-time asymptotic front shape.

A consequence of the above is that the total swept area decreases quite rapidly immediately after onset of an imposed pressure reduction, but can start to recover later on. To the extent that the area swept by the foam front gives an indication of the amount of gas currently in the system, this might show how net gas is injected into or extracted from a porous medium. It is also of interest to speculate whether total swept area might be held fixed were the injection pressure to be reduced gradually, rather than making a step change as was done here. Calculations like this have not been carried out here though: they require changes to the numerical implementation which currently treats regions above and below the neutral location independently.

It is necessary, however, to be cautious about associating swept area with the amount of gas present in the system. Pressure-driven growth even in its original forward-flow form does not describe a front separating pure gas from pure liquid. Instead it describes foamed gas (with a specified liquid saturation) on one side, and pure liquid on the other. In the case of reverse flow, there is instead foamed gas on both sides of the front, albeit with one side having slightly wetter foam than the other. The reverse foam front is not then very efficient at sweeping gas before it.

Only by solving a phase transport equation over the entire domain, and integrating the gas saturation, would the actual total amount of gas present at any instant be known. The fact that pressure-driven growth provides the front location but not the gas saturation field is certainly a limitation: swept area can only ever be a surrogate measure for the amount of gas present.

Another important point is that pressure-driven growth considers resistance to motion to be located at or near the foam front. This is again a recognized limitation of the model. Using the model to predict front velocity may be less reliable when resistance is spread out over a significant portion of the medium upstream or downstream of the front. This situation indeed can occur. In such cases, a Darcy-type model is needed. Furthermore, Darcy-type models might also be required (e.g. in cases involving driving liquid towards low-mobility foam) to predict whether or not viscous fingering instabilities are encountered. If fingering occurs, the front itself effectively becomes yet more spread out. In summary, pressure-driven growth is a simple way to explore interesting phenomena that could occur when foamed gas changes direction in a porous medium due to changes in injection pressure. However, for future work, it is relevant to ask whether those same phenomena would also be predicted by coupled Darcy-type and phase transport models, or whether instead different phenomena would be predicted.

Data accessibility. All results presented here are reproducible by procedures detailed in the article and the electronic supplementary material. Raw data analysed are also supplied as supplementary files.

Supplementary material are available online [62].

Declaration of AI use. We have not used AI-assisted technologies in creating this article.

Authors' contributions. P.G.: conceptualization, formal analysis, funding acquisition, investigation, methodology, software, writing—original draft; C.T.: conceptualization, formal analysis, funding acquisition, investigation, methodology, software, writing—review and editing; N.S.: formal analysis, writing—review and editing; S.A.: formal analysis, writing—review and editing.

All authors gave final approval for publication and agreed to be held accountable for the work performed therein.

Conflict of interest declaration. We declare we have no competing interests.

Funding. C.T.-U. acknowledges support from ANID Fondecyt Postdoctorado no. 3240010.

Acknowledgements. P.G. acknowledges discussions with I. Frigaard.

References

1. Rossen WR. 1996 Foams in enhanced oil recovery. In *Foams: theory, measurements and applications* (eds RK Prud'homme, SA Khan), Surfactant Science Series, pp. 99–187. New York: Marcel Dekker.
2. Farajzadeh R, Andrianov A, Krastev R, Hirasaki GJ, Rossen WR. 2012 Foam-oil interaction in porous media: implications for foam assisted enhanced oil recovery. *Adv. Colloid Interface Sci.* **183–184**, 1–13. (doi:10.1016/j.cis.2012.07.002)
3. Lake L, Johns RT, Rossen WR, Pope GA. 2014 *Fundamentals of enhanced oil recovery*, 2nd edn. Richardson, TX: Society of Petroleum Engineers.

4. Guo F, Aryana SA. 2016 An experimental investigation of nanoparticle-stabilized CO_2 foam used in enhanced oil recovery. *Fuel* **186**, 430–442. (doi:10.1016/j.fuel.2016.08.058)
5. Farajzadeh R, Bertin H, Rossen WR. 2020 Editorial to the special issue: foam in porous media for petroleum and environmental engineering: experience sharing. *Transp. Porous Media* **131**, 1–3. (doi:10.1007/s11242-019-01329-4)
6. Wang S, Mulligan CN. 2004 An evaluation of surfactant foam technology in remediation of contaminated soil. *Chemosphere* **57**, 1079–1089. (doi:10.1016/j.chemosphere.2004.08.019)
7. Bertin H, Del Campo Estrada E, Atteia O. 2017 Foam placement for soil remediation. *Environ. Chem.* **14**, 338–343. (doi:10.1071/EN17003)
8. Aranda R, Davarzani H, Colombano S, Laurent F, Bertin H. 2020 Experimental study of foam flow in highly permeable porous media for soil remediation. *Transp. Porous Media* **134**, 231–247. (doi:10.1007/s11242-020-01443-8)
9. Wang Z, Sun J, Wang Y, Guo H, Aryana SA. 2021 Optimum concentration of fly ash nanoparticles to stabilize CO_2 foams for aquifer and soil remediation. *J. Contam. Hydrol.* **242**, 103853. (doi:10.1016/j.jconhyd.2021.103853)
10. Hirasaki GJ, Miller CA, Szafranski R, Lawson JB, Akiya N. 1997a Surfactant/foam process for aquifer remediation. In *SPE Annual Technical Conference, San Antonio, TX, 18th–21st February*. (doi:10.2118/37257-MS).
11. Hirasaki GJ, Miller CA, Szafranski R, Tanzil D, Lawson JB, Meinardus H, Jin M, Londergan JT, Jackson RE, Pope GA, Wade WH. 1997b Field demonstration of the surfactant/foam process for aquifer remediation. In *SPE Annual Technical Conference and Exhibition, San Antonio, TX, 5th–8th October*. (doi:10.2118/39292-MS).
12. Longpré-Girard M, Martel R, Robert T, Lefebvre R, Lauzon JM, Thomson N. 2020 Surfactant foam selection for enhanced light non-aqueous phase liquids (LNAPL) recovery in contaminated aquifers. *Transp. Porous Media* **131**, 65–84. (doi:10.1007/s11242-019-01292-0)
13. Kovscek AR, Patzek TW, Radke CJ. 1995 A mechanistic population balance model for transient and steady-state foam flow in Boise sandstone. *Chem. Eng. Sci.* **50**, 3783–3799. (doi:10.1023/A:1010740811277)
14. Kovscek AR, Patzek TW, Radke CJ. 1997 Mechanistic foam flow simulation in heterogeneous and multidimensional porous media. *SPE J.* **2**, 511–526. (doi:10.2118/39102-PA)
15. Cheng L, Reme AB, Shan D, Coombe DA, Rossen WR. 2000 Simulating foam processes at high and low foam qualities. In *SPE Improved Oil Recovery Symposium, Tulsa, OK, 3rd–5th April*. (doi:10.2118/59287-MS).
16. Ma K, Ren G, Mateen K, Morel D, Cordelier P. 2015 Modeling techniques for foam flow in porous media. *SPE J.* **20**, 453–470. (doi:10.2118/169104-PA)
17. Zeng Y *et al.* 2016 Insights on foam transport from a texture-implicit local-equilibrium model with an improved parameter estimation algorithm. *Ind. Eng. Chem. Res.* **55**, 7819–7829. (doi:10.1021/acs.iecr.6b01424)
18. Guo F, Aryana SA. 2018 Improved sweep efficiency due to foam flooding in a heterogeneous microfluidic device. *J. Pet. Sci. Eng.* **164**, 155–163. (doi:10.1016/j.petrol.2018.01.042)
19. Portois C, Boeije CS, Bertin HJ, Atteia O. 2018 Foam for environmental remediation: generation and blocking effect. *Transp. Porous Media* **124**, 787–801. (doi:10.1007/s11242-018-1097-z)
20. Davarzani H, Aranda R, Colombano S, Laurent F, Bertin H. 2021 Experimental study of foam propagation and stability in highly permeable porous media under lateral water flow: diverting groundwater for application to soil remediation. *J. Contam. Hydrol.* **243**, 103917. (doi:10.1016/j.jconhyd.2021.103917)
21. Lawson JB, Reisberg J. 1980 Alternate slugs of gas and dilute surfactant for mobility control during chemical flooding. In *SPE/DOE Enhanced Oil Recovery Symposium, Tulsa, OK, 20th–23rd April*. (doi:10.2118/8839-MS).
22. Li RF, Yan W, Liu S, Hirasaki G, Miller CA. 2010 Foam mobility control for surfactant enhanced oil recovery. *SPE J.* **15**, 928–942. (doi:10.2118/113910-PA)
23. Zeng Y *et al.* 2020 Probing methane foam transport in heterogeneous porous media: an experimental and numerical case study of permeability-dependent rheology and fluid diversion at field scale. *SPE J.* **25**, 1697–1710. (doi:10.2118/199898-PA)
24. Føyen T, Brattekås B, Fernø MA, Barrabino A, Holt T. 2020 Increased CO_2 storage capacity using CO_2-foam. *Int. J. Greenhouse Gas Control* **96**, 103016. (doi:10.1016/j.ijggc.2020.103016)

25. Rossen WR, Farajzadeh R, Hirasaki GJ, Amirmoshiri M. 2024 Potential and challenges of foam-assisted CO_2 sequestration. *Geoenergy Sci. Eng.* **239**, 212929. (doi:10.1016/j.geoen.2024.212929)
26. Guo F, Aryana SA, Wang Y, McLaughlin JF, Coddington K. 2019 Enhancement of storage capacity of CO_2 in megaporous saline aquifers using nanoparticle-stabilized CO_2 foam. *Int. J. Greenhouse Gas Control* **87**, 134–141. (doi:10.1016/j.ijggc.2019.05.024)
27. Eneotu M, Grassia P. 2020 Foam improved oil recovery: towards a formulation for pressure-driven growth with flow reversal. *Proc. R. Soc. A* **476**, 20200573. (doi:10.1098/rspa.2020.0573)
28. Torres-Ulloa C, Grassia P. 2023 Foam propagation with flow reversal. *Transp. Porous Media* **147**, 629–651. (doi:10.1007/s11242-023-01925-5)
29. Shan D, Rossen WR. 2004 Optimal injection strategies for foam IOR. *SPE J.* **9**, 132–150. (doi:10.2118/88811-PA)
30. Heinemann N *et al.* 2021 Enabling large-scale hydrogen storage in porous media: the scientific challenges. *Energy Environ. Sci.* **14**, 853–864. (doi:10.1039/D0EE03536J)
31. Bunger AP, Lau H, Wright S, Schmidt H. 2023 Mechanical model for geomechanical pumped storage in horizontal fluid-filled lenses. *Int. J. Numer. Anal. Methods Geomech.* **47**, 1349–1372. (doi:10.1002/nag.3517)
32. Chavent G, Jaffré J. 1986 *Mathematical models and finite elements for reservoir simulation: single phase, multiphase and multicomponent flows through porous media*. Amsterdam, the Netherlands: Elsevier.
33. Chen Z, Ewing RE. 1997 Comparison of various formulations of three-phase flow in porous media. *J. Comput. Phys.* **132**, 362–373. (doi:10.1006/jcph.1996.5641)
34. Chen Z, Huan G, Ma Y. 2006 *Computational methods for multiphase flows in porous media*. Philadelphia, PA: Society for Industrial and Applied Mathematics.
35. de Paula FF, Igreja I, Quinelato T, Chapiro G. 2023 A numerical investigation into the influence of the surfactant injection technique on the foam flow in heterogeneous porous media. *Adv. Water Res.* **171**, 104358. (doi:10.1016/j.advwatres.2022.104358)
36. de Paula FF, Igreja I, Quinelato T, Chapiro G. 2024 Numerical simulation of foam displacement impacted by kinetic and equilibrium surfactant adsorption. *Adv. Water Res.* **188**, 104690. (doi:10.1016/j.advwatres.2024.104690)
37. de Velde Harsenhorst RM, Dharma AS, Andrianov A, Rossen WR. 2014 Extension of a simple model for vertical sweep in foam SAG displacements. *SPE Reservoir Eval. Eng.* **17**, 373–383. (doi:10.2118/164891-PA)
38. Grassia P, Mas-Hernández E, Shokri N, Cox SJ, Mishuris G, Rossen WR. 2014 Analysis of a model for foam improved oil recovery. *J. Fluid Mech.* **751**, 346–405. (doi:10.1017/jfm.2014.287)
39. Mas-Hernández E, Grassia P, Shokri N. 2015 Foam improved oil recovery: foam front displacement in the presence of slumping. *Colloids Surf. A, Physicochem. Eng. Aspects* **473**, 123–132. (doi:10.1016/j.colsurfa.2014.12.023)
40. Mas-Hernández E, Grassia P, Shokri N. 2015 Foam improved oil recovery: modelling the effect of an increase in injection pressure. *Eur. Phys. J. E* **38**, 67. (doi:10.1140/epje/i2015-15067-6)
41. Grassia P, Torres-Ulloa C, Berres S, Mas-Hernández E, Shokri N. 2016 Foam front propagation in anisotropic oil reservoirs. *Eur. Phys. J. E* **39**, 42 (doi:10.1140/epje/i2016-16042-5)
42. Mas-Hernández E, Grassia P, Shokri N. 2016 Modelling foam improved oil recovery within a heterogeneous reservoir. *Colloids Surf. A, Physicochem. Eng. Aspects* **510**, 43–52. (doi:10.1016/j.colsurfa.2016.07.064)
43. Grassia P, Lue L, Torres-Ulloa C, Berres S. 2017 Foam front advance during improved oil recovery: similarity solutions at early times near the top of the front. *J. Fluid Mech.* **828**, 527–572. (doi:10.1017/jfm.2017.541)
44. Grassia P. 2018 Pressure-driven growth in strongly heterogeneous systems. *Eur. Phys. J. E* **41**, 10. (doi:10.1140/epje/i2018-11618-7)
45. Torres-Ulloa C, Berres S, Grassia P. 2018 Foam-liquid front motion in Eulerian coordinates. *Proc. R. Soc. A* **474**, 20180290. (doi:10.1098/rspa.2018.0290)
46. Torres-Ulloa C, Grassia P. 2021 Breakdown of similarity solutions: a perturbation approach for front propagation during foam improved oil recovery. *Proc. R. Soc. A* **477**, 20200691. (doi:10.1098/rspa.2020.0691)
47. Zhou Z, Rossen WR. 1995 Applying fractional-flow theory to foam processes at the limiting capillary pressure. *SPE Adv. Technol. Ser.* **3**, 154–162. (doi:10.2118/24180-PA)

48. Buckley SE, Leverett MC. 1942 Mechanism of fluid displacement in sands. *Trans. AIME* **146**, 107–116. (doi:10.2118/942107-G)
49. Dholkawala ZF, Sarma HK, Kam SI. 2007 Application of fractional flow theory to foams in porous media. *J. Pet. Sci. Eng.* **57**, 152–165. (doi:10.1016/j.petrol.2005.10.012)
50. Ashoori E, van der Heijden T, Rossen WR. 2010 Fractional-flow theory of foam displacements with oil. *SPE J.* **15**, 260–273. (doi:10.2118/121579-PA)
51. Zhou ZH, Rossen WR. 1994 Applying fractional-flow theory to foams for diversion in matrix acidization. *SPE Prod. Facil.* **9**, 29–35. (doi:10.2118/24660-PA)
52. Li S, Li Z, Lin R, Li B. 2008 Research and application of mathematical model for foam diversion acidizing. In *SPE Western Regional and Pacific Section AAPG Joint Meeting, Bakersfield, CA, 29th March–2nd April*. (doi:10.2118/114003-MS)
53. Gong JK, Wang Y, Bahrim RZBK, Tewari RD, Amir MIM, Farajzadeh R, Rossen W. 2024 Liquid injectivity in a SAG foam process: effect of permeability. *Pet. Sci.* **21**, 302–314. (doi:10.1016/j.petsci.2023.10.010)
54. Saffman PG, Taylor GI. 1958 The penetration of a fluid into a porous medium or Hele-Shaw cell containing a more viscous liquid. *Proc. R. Soc. Lond. A* **245**, 312–329. (doi:10.1098/rspa.1958.0085)
55. Homsy GM. 1987 Viscous fingering in porous media. *Annu. Rev. Fluid Mech.* **19**, 271–311. (doi:10.1146/annurev.fl.19.010187.001415)
56. Wang Y, Mckinzie J, Furtado F, Aryana SA. 2018 Analysis of nonequilibrium effects and flow instability in immiscible two-phase flow in porous media. *Adv. Water Res.* **122**, 291–303. (doi:10.1016/j.advwatres.2018.10.019)
57. Wang Y, Aryana SA, Furtado F, Ginting V. 2020 Scaling analysis of two-phase flow in fractal permeability fields. *Water Resour. Res.* **56**, e2020WR028214. (doi:10.1029/2020WR028214)
58. Yortsos YC, Hickernell FJ. 1989 Linear stability of immiscible displacement in porous media. *SIAM J. Appl. Math.* **49**, 730–748. (doi:10.1137/0149043)
59. King MJ, Dunayevsky VA. 1989 Why waterflood works: a linearized stability analysis. In *SPE Annual Technical Conference and Exhibition, San Antonio, TX, 8th–11th October*. (doi:10.2118/SPE-19648-MS)
60. Maas JG, Springer N, Hebing A, Snippe J, Berg S. 2024 Viscous fingering in CCS: a general criterion for viscous fingering in porous media. *Int. J. Greenhouse Gas Control* **132**, 104074. (doi:10.1016/j.ijggc.2024.104074)
61. Courant R, Friedrichs KO. 1976 *Supersonic flow and shock waves*. New York, NY: Springer.
62. Grassia P, Torres-Ulloa C, Shokri N, Aryana S. 2025 Pressure-driven growth with forward and reverse foam flow: modelling foam flow in geological formations. Figshare. (doi:10.6084/m9.figshare.c.7819490)